Corrosion Science 249 (2025) 112849

Contents lists available at ScienceDirect

Corrosion Science

journal homepage: www.elsevier.com/locate/corsci

Understanding the effect of oxide ions on Solar Salt chemistry and corrosion mechanism of 316 L stainless steel at 600 °C

Sumit Kumar [a,*,1], Srinivasan Swaminathan [b,1], Rene Hesse [b], Hennig Goldbeck [b], Wenjin Ding [a], Alexander Bonk [c], Thomas Bauer [d]

[a] German Aerospace Center (DLR), Institute of Engineering Thermodynamics, Stuttgart 70569, Germany
[b] Bundesanstalt für Materialforschung und -prüfung (BAM), Department of Materials Engineering, Division 5.1 – Microstructural Design and Degradation, Unter den Eichen 87, Berlin 12205, Germany
[c] Drees & Sommer, Obere Waldplätze 13, Stuttgart 70569, Germany
[d] German Aerospace Center (DLR), Institute of Engineering Thermodynamics, Cologne 51147, Germany

ARTICLE INFO

Keywords:
Solar Salt
Austenitic stainless steel
Alkali oxides
Corrosion mechanism
Thermal Energy Storage
High temperature corrosion

ABSTRACT

Solar Salt (60 wt% $NaNO_3$,40 wt% KNO_3), used in Concentrated Solar Power (CSP) Thermal Energy Storage (TES) technology, can decompose into various products at elevated temperatures, with oxide ions being one of the known corrosive byproducts. The study mimics Solar Salt aging by intentionally adding sodium peroxide (Na_2O_2) and sodium oxide (Na_2O) at concentrations of 0.005–0.33 wt% to investigate their role in the corrosion of austenitic stainless steel at 600°C in typical operating conditions. Salt chemistry (nitrite, nitrate, oxide ions, and metal cations) was analyzed every 24 h, and steel corrosion after 168 h was assessed by weight change, corrosion rate, phase analysis, and cross-sectional morphology. Results reveal that at or above 0.135 wt% added Na_2O_2/Na_2O leads to a quasi-steady-state equilibrium of oxide ions in the salt. Interestingly, at these concentrations, the presence of steel further decreases oxide ion concentration. Furthermore, above 0.135 wt%, the corrosion rate increases significantly, along with increased spallation, porosity and disintegration of the corrosion layer, forming a non-protective layer. This study highlights the critical role of oxide ions in the corrosion process.

1. Introduction

A globally increasing energy demand coupled with a growing concern for reducing carbon emissions has promoted numerous advancements in the adoption of renewable energy. One of the major advancements is the Concentrated Solar Power (CSP) to capture solar energy for power generation. Thermal Energy Storage (TES), historically integrated with CSP plants, promotes the flexible utilization of intermittent solar energy. The use of non-eutectic nitrate salt mixture (60 wt % $NaNO_3$/40 wt% KNO_3) as a heat storage medium is currently virtually in all CSP plants the standard commercial TES technology [1]. The nitrate salt mixture, commonly known as Solar Salt, offers several advantages, including high density, high heat capacity, low vapor pressure, low cost, non-toxicity, non-flammability, and minimal environmental impact. It operates at a state-of-the-art temperature of 560 °C [2]. It is widely acknowledged that above 500 °C, Solar Salt undergoes several reversible decomposition reactions, with one of the commonly observed reactions involving the decomposition of nitrate ions into nitrite ions and oxygen gas as shown in Eq. 1. Under typical operating conditions, in an air atmosphere with an oxygen partial pressure of 0.20 atm, the nitrite content can reach approximately 4.5 mol% at 560 °C [3–6].

$$NO_3^- \rightleftarrows NO_2^- + \frac{1}{2}O_2(g) \quad (1)$$

Further decomposition of nitrite ions can lead to the generation of various nitrogen oxide (N_xO_y) gases (N_2O, NO_2, NO or also N_2) and different oxide ions (O_a^{b-}) typically dissolved in the salt melt (e.g. O^{2-}, O_2^{2-}, O_2^-), as shown in Eq. 2. A generalized equation is used hereafter, as the decomposition reactions are complex and not fully understood yet [7–9]. Under typical operating conditions for CSP-TES in atmospheric air, the absence of N_xO_y gases allows the concentration of oxide ions to

* Corresponding author.
E-mail address: Sumit.kumar@dlr.de (S. Kumar).
[1] Authors contributed equally.

https://doi.org/10.1016/j.corsci.2025.112849
Received 12 December 2024; Received in revised form 11 February 2025; Accepted 6 March 2025
Available online 11 March 2025

increase over time, by shifting the equilibrium of Eq. 2 toward the product side. Several studies have shown that in the absence of N_xO_y gases, the oxide ion concentration in Solar Salt can exceed 0.08 mol% at 600 °C after 1000 h in synthetic air [8,10]. Steinbrecher et al. [11] demonstrated that the addition of 1 mol% sodium peroxide to Solar Salt in synthetic air at 600 °C does not impact the long-term nitrate and nitrite decomposition reaction (Eq. 1), stabilizing at a 90/10 mol% nitrate/nitrite ratio. However, the overall oxide ion concentration in Solar Salt decreases initially and stabilizes at a lower level after 1000 h.

$$NO_2^- \rightleftarrows N_xO_y(g) + O_a^{b-} \quad (2)$$

Oxide ions produced from the decomposition reaction are known to be corrosive in nature and can oxidise alloys in contact [12,13]. Earlier studies by Slusser et al. [14] have shown that the addition of 0.1–1 mol% sodium peroxide(Na_2O_2) impurity to the equimolar $NaNO_3/KNO_3$ salt mixture can increase the corrosion rate of AISI 316 steel by 30 times, reaching to 965 μm/year after 14 days at 650°C. Furthermore, Federsel et al. [15] demonstrated an escalation in the corrosion rate when a 1 wt % sodium oxide(Na_2O) impurity was introduced to the molten nitrate/nitrite salt mixture at 530°C. Marchiano et al. [16,17] indicated that exceeding a specific oxide ions concentration threshold in a nitrate melt at 330 °C lead to the breakaway of the passive corrosion layer formed on the metal. Similarly, Fontana et al. [18] also highlighted that elevating the concentration of any corrosive species beyond a certain level can intensify the corrosion process. Our previous research on Solar Salt corrosion at 600 °C showed that increased oxide ion concentration from salt decomposition, influenced by the cover gas atmosphere, leads to a porous, non-protective corrosion layer, accelerating corrosion. Additionally, oxide ion consumption follows a pattern in presence of steel between 0.06 and 0.24 wt% [19]. In our recent work, we also found that adding sodium oxide (Na_2O) to Solar Salt above 0.135 wt% at 600 °C in air leads to increased corrosion in AISI 316 L and also changes the structural morphology of the formed corrosion layers [20]. While that study highlighted the critical concentration of oxide ions and the resulting impact on corrosion morphology, its focus was limited to the role of sodium oxide (Na_2O) in influencing metallic corrosion and did not include any analysis of salt chemistry. Understanding the involvement and evolution of the salt chemistry is crucial for depicting the comprehensive corrosion process.

This study builds upon and significantly extends the scope of our previous findings by examining two types of oxide impurities, namely sodium oxide (Na_2O) and sodium peroxide (Na_2O_2). Additionally, for the first time, it provides an in-depth analysis of salt chemistry with and without steel, focusing on the interactions of nitrate, nitrite, and oxide ions in the corrosion process. The principal goal of the current study is not only to identify the critical concentration of oxide ions beyond which the corrosiveness of the salt experiences a significant increase, but also to investigate the change in salt chemistry in relation to corrosion, contribute to a better understanding of the underlying corrosion mechanism. In this work, austenitic stainless steel AISI 316 L is tested under extreme conditions at 600°C. While the typical operating temperature for Solar Salt in CSP applications is below 565°C, there is growing interest in exploring higher temperatures to enhance energy storage density, reduce storage capital expenditure, and improve the thermal to electrical conversion efficiency of the power cycle. This study also aims to simulate the long-term aging of Solar Salt by creating an oxide ion-rich composition. To achieve this, sodium oxide (Na_2O) and sodium peroxide (Na_2O_2), were added at concentrations ranging from 0.005 to 0.33 wt% over a short duration of 168 h. This approach mimics the impact of oxide ion accumulation on metallic components in contact with Solar Salt over extended periods. Overall, this study analyzes the allowable oxide ions concentration in the Solar Salt at 600 °C for the metallic components in CSP and offers deeper insights into the corrosion mechanism with increasing oxide ions concentration in the Solar Salt. This novel systematic approach contributes to our understanding of the role of oxide ions in CSP-TES systems corrosion, paving the way for advancements in corrosion control and providing valuable insights into optimizing system performance.

2. Materials and methods

This study investigates different levels of sodium oxide and sodium peroxide impurities, ranging from 0.005 wt% to 0.33 wt%, added to Solar Salt. The corrosion test was conducted on AISI 316 L, a commonly used stainless-steel in CSP-TES, under test condition of 600 °C over a period of 168 h(7days) in synthetic air. In the same setup, reference experiments without steel were carried out under equivalent oxide ion impurity levels to analyze and compare the resultant changes in the salt chemistry with and without steel (see Subsection 2.1 and 2.2).

The chemistry of the Solar Salt was examined using Ion Chromatography (IC), titration, and Microwave Plasma Atomic Emission Spectrometry (MP-AES) (see Subsection 2.3.1). The post analysis of the steel corrosion involved weight change measurements after corrosion test, mass loss assessment through descaling, Scanning Electron Microscopy with Energy Dispersive X-ray Spectroscopy (SEM-EDX), and X-ray Diffraction (XRD) (see Subsection 2.3.2).

2.1. Experimental setup

The corrosion experiment was performed in alumina crucibles with an alumina sample holder to exclude the interaction of Solar Salt with any metallic components of the setup. Fig. 1 illustrates the schematic of the experimental setup, which is similar to the setup described in detail elsewhere [21]. A modified convection furnace with circular holes on the top was used for heating. To prevent salt from creeping outside the alumina crucible and to facilitate easy handling of the salt samples, these crucibles extended deliberately approximately 30 mm outside the furnace. The atmosphere inside the crucibles were maintained by using a steel flange assembly on the top of the alumina crucibles. The steel flanges were made with three holes on the top: two for gas inlet and outlet, and the one for thermocouple insertion. A K-type thermocouple with alumina covering, fully immersed in the salt throughout the experiment, was utilized to monitor the salt temperature. The steel samples were assembled in an alumina sample holder and this holder was placed inside the alumina crucible. Mass flow controllers (MFCs) were used to precisely maintain the gas atmosphere above the salt in all crucibles. Synthetic air (80 % N_2 (grade 5.0)/ 20 % O_2(grade 5.0), Linde gas, Germany) was used at a Flow rate of 100 mL/min. The reference experiments were also carried out in the same setup without the steel samples.

2.2. Experimental procedure

For the corrosion test the Solar Salt was produced from pro analysis grade $NaNO_3$ (purity >99.5 %, Merck, Germany) and KNO_3 (purity >99.5 %, Merck, Germany) at a 60/40 wt% ratio. Sodium oxide (purity 80 % Na_2O, remaining 20 % Na_2O_2, Merck, Germany) was added to the Solar Salt at six different concentrations. Similarly, sodium peroxide (Na_2O_2, purity >97 %, Merck, Germany) was added at six different concentrations. The corrosion tests were conducted with stainless steel AISI 316 L (Outokumpu, Germany), and reference experiments were performed without steel for each of the six concentrations of added sodium oxide and sodium peroxide. The chemical composition of the 316 L austenitic stainless steel (in wt%) listed in Table 1, was obtained using the spark emission spectrometer (SPECTROLAB S, AMETEK). The experiment labeling scheme is determined by the type of oxide (1), the amount of added oxide impurity (2), and the presence or absence of steel (3), as depicted in Fig. 2.

For the sodium oxide added Solar Salt corrosion experiments, 100 g of Solar Salt were mixed with six different concentrations of sodium oxide, each filled into separate alumina crucible. The same procedure

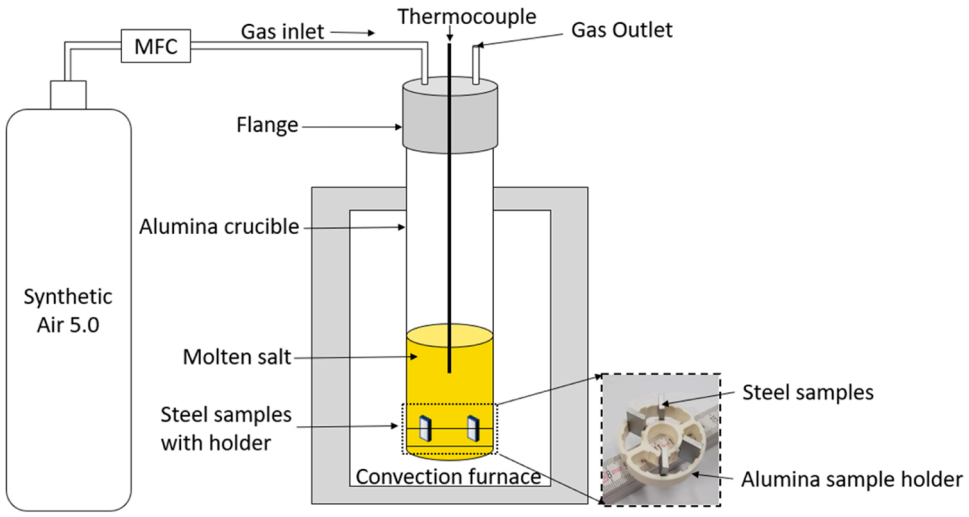

Fig. 1. Schematic diagram of the experimental setup for the corrosion test, including the convection furnace with an alumina crucible and alumina sample holder.

Table 1
Elemental composition (wt%) of the AISI 316 L austenitic steel used in this study, obtained through the spark emission spectrometer (remaining Fe and few other minor elements).

C %	Cr %	Ni %	Si %	Mn %	Cu %	P %	S %	Mo %	N %
0.02	17.1	10.1	0.52	0.87	0.49	0.03	< 0.001	2.04	0.04

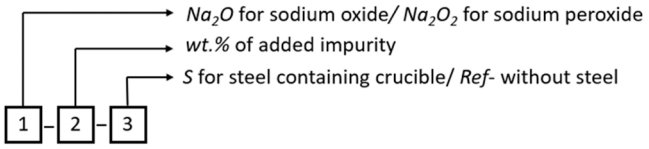

Fig. 2. Experiment labeling according to added sodium oxide or sodium peroxide impurity and steel sample.

was applied for the sodium peroxide experiments. Since sodium oxide and sodium peroxide is hydroscopic in nature the preperation of the salt mixtures was carried out in the Glove Box (GS Glovebox System Technik GmbH, Glovebox Mega 2, $O_2 < 0.5$ ppm, $H_2O < 1$ ppm). Austenitic stainless steel AISI 316 L samples (see Table 1 for composition) were prepared by cutting them in a uniform size of 20 × 10 x 3 mm followed by grinding with SiC paper down to P600 grit, and then finally washed with deionized water and acetone. In total 12 steel samples (see Table 2) were arranged in six alumina sample holders with two steel samples per crucible.

The six-sample holders were arranged in six different alumina crucibles with different sodium oxide concentrations namely 0.005 wt%, 0.070 wt%, 0.135 wt%, 0.200 wt%, 0.265 wt% and 0.330 wt%. Experiment labeling, based on the type and quantity of added oxide impurity, as well as post-analysis methods for both steel-containing and reference crucibles, can be found in Table 2. The crucibles were heated to 600°C and kept for 168 h (7 days) at 600 °C. During the test, initial salt samples were drawn at t = 0 h, once the salt temperature reached 600°C, and additional samples were collected every 24 h until 168 h. Reference experiments were also conducted without steel to analyze changes in salt chemistry with varying concentrations of sodium oxide. The same procedure was followed for sodium peroxide added to Solar Salt. After the 168-hour corrosion test, steel samples were extracted from the steel containing crucibles. Details on salt and steel post analysis follow in the next subchapter and are explained separately.

2.3. Post-analysis techniques

2.3.1. Salt analysis

The salt samples collected from each crucible with steel and without steel for each oxide ion concentration at every 24 h were analyzed for multiple anions (nitrate, nitrite, and oxide) and dissolved metal cations in the salt (iron, chromium, and nickel).

Salt samples were analyzed using ion chromatography (IC) (Metrohm model 880 Basic IC plus, Germany) for nitrate, nitrite, and chromate ions. For ion chromatography 125 mg of salt was dissolved in 500 mL ultra-pure water and analyzed. The detailed description of the experiment and calibration is given elsewhere [22].

Acid-base titration (Metrohm Titrando 800, Herisau, Switzerland) was performed to find the oxide ions concentrations in the salt. 500 mg of salt was dissolved in around 160 mL water and titrated with 0.01 M HCl (Titrisol standard solution). To find the exact concentration of HCl in the titration solution, titer determination was performed against sodium carbonate (Merck, Germany, purity >99.5 %). The concentration of oxide ions measured through titration is generally depicted as O^{2-}, regardless of the specific oxide species present in the Solar Salt. The analysis techniques and statistical analysis of titration methods are described elsewhere in detail [11].

Microwave plasma atomic emission spectrometry (MP-AES) (Agilent Technologies G8007AA, Germany) was done to analyze the metal cation content in the salt mixture. Calibration was performed using an ICP multielement standard solution (Merck, Germany) at different concentrations ranging from: 0.1–10 mg/L. To the calibration solutions 1 % HNO_3 and 1 % of pure Solar Salt were added. The samples were prepared by dissolving 1 % salt in a 1 % HNO_3 solution. The concentrations of Fe, Ni, and Cr were then measured by normalizing the detected intensities with the mass of salt added.

2.3.2. Steel analysis

Two steel samples were extracted from each crucible with different oxide impurities and analysed as follows.

Table 2
Experiment matrix including experiment notation, utilized crucible number, steel type and post analysis techniques for steel and salt samples.

Crucible number	Added oxide (wt%) and type	Experiment notation (see Fig. 2)	Post analysis of steel	Post analysis of salt
1	0.005 Na_2O	Na_2O−0.005 wt%-S		
2	0.005 Na_2O_2	Na_2O_2−0.005 wt%-S		
3	0.070 Na_2O	Na_2O−0.070 wt%-S		
4	0.070 Na_2O_2	Na_2O_2−0.070 wt%-S		
5	0.135 Na_2O	Na_2O−0.135 wt%-S		
6	0.135 Na_2O_2	Na_2O_2−0.135 wt%-S	316 L Sample 1: Weight change and mass loss	IC, titration,
7	0.200 Na_2O	Na_2O−0.200 wt%-S	316 L Sample 2: SEM-EDX, XRD	MP-AES
8	0.200 Na_2O_2	Na_2O_2−0.200 wt%-S		
9	0.265 Na_2O	Na_2O−0.265 wt%-S		
10	0.265 Na_2O_2	Na_2O_2−0.265 wt%-S		
11	0.330 Na_2O	Na_2O−0.330 wt%-S		
12	0.330 Na_2O_2	Na_2O_2−0.330 wt%-S		
1	0.005 Na_2O	Na_2O−0.005 wt%-ref		
2	0.005 Na_2O_2	Na_2O_2−0.005 wt%-ref		
3	0.070 Na_2O	Na_2O−0.070 wt%-ref		
4	0.070 Na_2O_2	Na_2O_2−0.070 wt%-ref		
5	0.135 Na_2O	Na_2O−0.135 wt%-ref		
6	0.135 Na_2O_2	Na_2O_2−0.135 wt%-ref		IC, titration
7	0.200 Na_2O	Na_2O−0.200 wt%-ref		
8	0.200 Na_2O_2	Na_2O_2−0.200 wt%-ref		
9	0.265 Na_2O	Na_2O−0.265 wt%-ref		
10	0.265 Na_2O_2	Na_2O_2−0.265 wt%-ref		
11	0.330 Na_2O	Na_2O−0.330 wt%-ref		
12	0.330 Na_2O_2	Na_2O_2−0.330 wt%-ref		

- Sample 1: Weight change after corrosion, and corrosion rate after descaling.
- Sample 2: The corrosion layer phases were analyzed using X-ray Diffraction (XRD), and the chemistry was examined using Scanning Electron Microscopy with Energy Dispersive X-ray Spectroscopy (SEM-EDX) and Focused Ion Beam with Energy Dispersive X-ray Spectroscopy (FIB-EDX).

The detail explanation of each analysis is provided below.

The steel samples were extracted after 168 h. First the samples were cleaned with deionized water, dried overnight, and weighted to get the area specific weight change(mg/cm^2). The area specific weight change was calculated as per Eq. 3.

$$\Delta w = \frac{m_c - m_i}{S_0} \tag{3}$$

Where Δw is the weight change per unit area (mg/cm^2), m_c is the final sample mass after washing with deionized water following the corrosion test in (mg), m_i is the initial sample mass in (mg) and S_0 is the initial sample surface area in (cm^2).

To determine the corrosion rate (μm/year), the descaling was done as described in ASTM G1(C7.4). The descaling process was repeated for 8–10 successive cycles until a steady mass loss was achieved. The mass loss per unit area was calculated according to Eq. 4.

$$\Delta m = \frac{m_f - m_i}{S_0} \tag{4}$$

Where Δm is the descaled mass loss per unit area (mg/cm^2), m_f is the final sample mass after descaling in (mg). The corrosion rate per year was further calculated by linear extrapolation of 168 h corrosion test as per Eq. 5.

$$CR\left(\frac{\mu m}{y}\right) = \frac{87600 * \Delta m}{t * \rho} \tag{5}$$

Where Δm is the mass loss per unit area calculated from Equation 4, t is time of corrosion test (168 h) and ρ is the density of steel (7.93 g/cm^3).

As post-exposure analysis of the steel samples, the XRD analysis for phase identification of the corrosion products was performed, in Grazing Incidence X-ray diffraction (GI-XRD) mode. The samples that were tested in 0.005, 0.07, 0.135, 0.2 wt% Na_2O as well as Na_2O_2-added Solar Salt were measured using Seifert XRD 3000 PTS equipped with Co X-ray source, whereas the samples tested at higher concentration of oxide/peroxide impurities (such as 0.265 and 0.33 wt%) were measured in STOE (STADI MP) multipurpose XRD installed with Mo X-ray source. Both the diffractometers were configured with 1.5° incident angle, and the measurements were recorded at 2θ values from 15 to 80° with a 10 s count time. To identify the formed phases of the corrosion products, all the measured patterns were plotted in scattering vector ($Q = (4\pi/\lambda)\sin(\theta)$, where θ is the Bragg angle and λ is the wavelength of the X-ray source), and then, compared to the known patterns in ICSD (Inorganic Crystal Structure Database).

The cross-sections of the corrosion products formed on the steel samples that were tested in 0.005–0.2 wt% Na_2O or Na_2O_2-added Solar Salt were examined using Scanning Electron Microscopy (SEM - Tescan Vega3), and their elemental analyses were carried out in an Energy Dispersive X-ray spectroscopy (EDX). For this cross-sectional analysis, the samples were embedded in an epoxy resin followed by an appropriate grinding and polishing. Before mounting in resin, a sputtered Au coating followed by the electrochemically deposited Ni coating were applied on the samples to protect the corrosion layer from grinding/polishing processes.

The samples exposed to 0.265 and 0.33 wt% Na_2O or Na_2O_2 added Solar Salt were cross-sectioned using dual beam Focused Ion Beam (FEI-FIB Quanta 3D FEG) due to the fragility of the corrosion layer. After FIB-milling completion, the corrosion layer was analyzed using EDX integrated with the FIB-machine. This FIB-cut approach is helpful, in particular, where the corrosion layers are very fragile and prone to spallation.

3. Results

In this section, the salt chemistry for Na_2O_2- and Na_2O-added Solar Salt, with and without steel, is discussed in Section 3.1, followed by the steel corrosion results in Section 3.2.

3.1. Salt analysis

3.1.1. Sodium peroxide impact on salt chemistry without steel

To evaluate the impact of added sodium peroxide (Na_2O_2) on Solar

Salt chemistry, this subsection specifically discusses the salt chemistry of the reference experiment with increasing added sodium peroxide, conducted without the steel samples. The impact of added sodium oxide on Solar Salt chemistry (Section 3.1.3) is also presented and discussed in a similar manner to this section.

The discussion initially focuses on the change in oxide(O^{2-}) ion content measured through titration in the reference experiment over the course of 168 h. Subsequently, the variation in nitrate (NO_3^-) and nitrite (NO_2^-) ion measured through ion chromatography is presented and discussed.

The oxide ions concentrations, measured every 24 h through acid-base titration, are presented in Fig. 3(a) with open symbols denoting the reference experiment conducted without steel samples. For clarity, the added sodium peroxide concentrations are depicted in wt% related to the overall salt mass, while the measured oxide ions concentration from titration are shown as mol% of all anions.

At 0.005 wt% added sodium peroxide in Solar Salt, the overall oxide ions concentration in the salt remains below the detection limit (<0.01 mol%) at t = 0. However, over time, the concentration gradually increases, reaching a final value of 0.035 mol% at 168 h. These observations align with trends reported in the literature, where oxide ion concentrations in Solar Salt under purged synthetic air conditions at 600 °C, without any oxide addition, remain below 0.01 mol% within the first 200 h [10]. By 1000 hours of salt exposure at 600 °C, the oxide ion concentration increases and typically reaches around 0.5 mol% [10,19]. At 0.070 wt% added sodium peroxide, the initial concentration is 0.061 mol% and increases to 0.097 mol% at 168 h. For 0.135 wt% added sodium peroxide, the initial oxide ions concentration is 0.124 mol % and rises to 0.142 mol%. At 0.200 wt% added sodium peroxide, the concentration starts at 0.196 mol% and increases to 0.206 mol%. For 0.265 wt% added sodium peroxide, the concentration starts at 0.292 mol% and remains steady at 0.257 mol% at 168 h. Finally, at 0.330 wt% sodium peroxide, the concentration starts at 0.342 mol% and remains steady around 0.280 mol%. At low added sodium peroxide concentration of 0.005 wt%, 0.070 wt%, and 0.135 wt% the oxide ions concentration in the salt increases over time and do not appear to reach a steady-state most probably due to the absence of nitrogen oxide gases in the purge gas, as shown in Eq. 2. The absence of nitrous gases can push the equilibrium to the right side of the reaction 2, leading to more oxide ions formation over time [8]. However, the addition of 0.200 wt%, 0.265 wt%, and 0.330 wt% sodium peroxide results in a smaller increase or fluctuation in the overall concentration of oxide ions in the salt compared to the lower concentrations. This may suggest the potential establishment of a quasi-steady-state equilibrium, possibly involving interactions with nitrite and nitrate ions, as discussed by Zambonin et al. [23], or the potential involvement of added oxide ions in suppressing the decomposition reaction described in Eq. 2. A detailed analysis of this phenomenon, however, falls beyond the scope of the current investigation.

The nitrate and nitrite anion content measured for the reference samples through IC are shown in Fig. 3(b). At t = 168 h, regardless of the sodium oxide impurity concentration (ranging from 0.005 wt% to 0.330 wt%), the nitrate/nitrite content stabilized around 89.6/10.2 mol %. This observation aligns with the previously discussed equilibrium data by Nissen and Meeker, which state nitrate/nitrite equilibrium content of 90/10 mol% under air atmosphere at 600°C [3]. It also suggests that the addition of sodium peroxide does not significantly alter the nitrate/nitrite equilibrium over the long term.

3.1.2. *Sodium peroxide impact on salt chemistry with steel*

To analyze the effect of increasing added sodium peroxide (Na_2O_2) concentrations in the presence of steel on the overall oxide ions concentration in the salt, Fig. 3(a) depicts the variation in oxide ions concentration over time. Filled symbols represent the oxide ions concentration in steel-containing experiments.

At 0.005 wt% added sodium peroxide, the concentration remains below the detection limit (<0.01 mol%) at t = 0 and increases to 0.122 mol% at 168 h. For 0.070 wt% added sodium peroxide, it increases from 0.061 mol% to 0.112 mol% at 168 h. At 0.135 wt%, it rises from 0.125 mol% to 0.135 mol%. For 0.200 wt%, it slightly decreases from 0.200 mol% to 0.156 mol%. At 0.265 wt%, the concentration also decreases from 0.268 mol% to 0.231 mol%. For 0.330 wt%, it decreases from 0.327 mol% to 0.269 mol%. Comparing these results with the reference crucible without steel, at a low concentration of 0.005 wt% sodium peroxide, there is an increase in oxide ions concentration in the steel-containing salt samples. At and above 0.135 wt%, a decrease in oxide ions concentration is observed in the steel-containing salt samples compared to the reference experiments. This difference indicates the role of steel in decreasing the overall oxide ions in the Solar Salt. A detailed discussion on the variation of oxide ions concentrations with and without steel will be provided in Section 4, after discussing the individual impacts of added sodium peroxide and sodium oxide on steel corrosion in Solar Salt.

The nitrate and nitrite anion content measured for the reference samples through IC are shown in Fig. 3(b). At t = 168 h, regardless of the sodium oxide impurity concentration (ranging from 0.005 wt% to 0.330 wt%), the nitrate/nitrite content stabilized around 90.1/9.7 mol %. This observation aligns with the previously discussed equilibrium

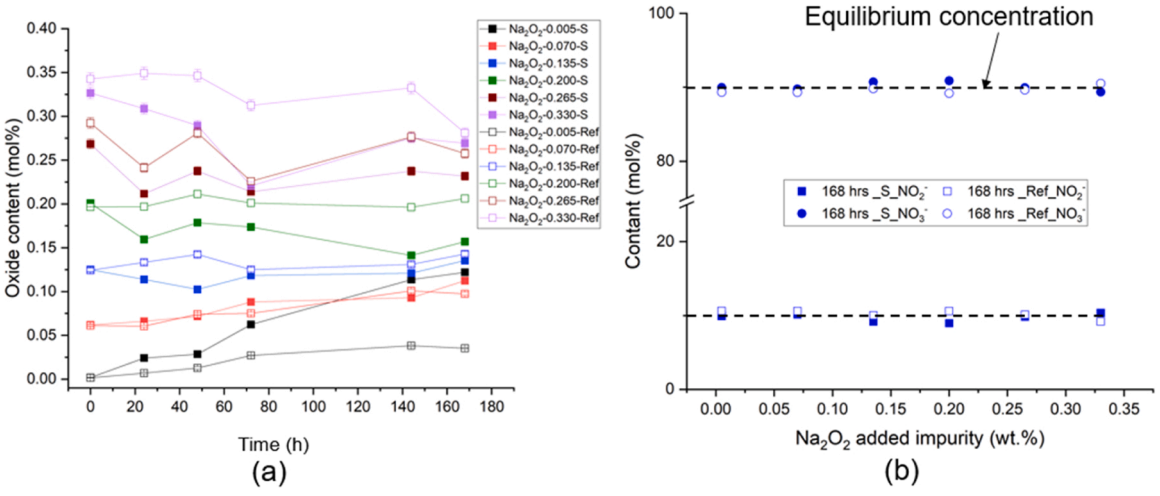

Fig. 3. Anion contents in Solar Salt at 600 °C with Na_2O_2 added impurity a) Oxide ions concentration in Solar Salt measured from acid-base titration (error bars not visible are in the symbol size) b) Nitrate/nitrite content in Solar Salt measured through ion chromatography after 168 h of exposure.

from Eq. 1. Additionally, these findings are similar to those observed when steel was not present in the salt, suggesting that the presence of steel does not significantly affect the nitrate/nitrite equilibrium in long term with the added sodium peroxide concentrations.

To identify and evaluate the variation in metal concentration resulting from the presence of steel in Solar Salt with increasing amounts of added sodium peroxide, MP-AES analysis was performed on the salt samples after 168 h of exposure. The results are presented in Fig. 4, where the concentrations (in PPM by weight) of iron (Fe), chromium (Cr), and nickel (Ni) are plotted against increasing sodium peroxide concentration. The chromium (Cr) concentration increases with the addition of sodium peroxide in Solar Salt, rising from 9 PPM at 0.005 wt % to 136 PPM at 0.33 wt%. Iron (Fe) also shows an initial increase from 1 PPM at 0.005 wt% to 59 PPM at 0.200 wt% added sodium peroxide, followed by a decrease to 8 PPM at 0.330 wt%. Nickel (Ni) remains relatively stable, with 9 PPM at 0.005 wt% and 1 PPM at 0.330 wt%. The results at 0.005 wt% added sodium peroxide are consistent with earlier research, where the absence of added oxide impurities led to very low concentrations of Fe and Ni (<1 PPM) and approximately 50 PPM of Cr within the first 200 hours of corrosion testing under synthetic air at 600 °C [19]. Overall, an increase in Cr and Fe concentrations in the salt is observed as the sodium peroxide concentration in Solar Salt increases, particularly after adding 0.135 wt% sodium peroxide. Additionally, an uneven distribution of dark brown particles was observed in the salt after the corrosion experiment, likely containing metals released from the corrosion of steel. These particles appear in greater quantities at higher sodium peroxide concentrations, which may affect the consistency of the measurements and could explain the abrupt increase of iron (Fe) observed at 0.20 wt% added sodium peroxide in the salt.

3.1.3. Sodium oxide impact on salt chemistry without steel

To analyze the impact of added sodium oxide (Na_2O) on Solar Salt chemistry, this subsection presents and discusses the salt chemistry of the reference experiment, conducted without the steel samples.

The oxide ions(O^{2-}) concentration, measured every 24 h through acid-base titration, are presented in Fig. 5(a), with open symbols denoting the reference experiment conducted without steel samples. The results are presented, starting from a low sodium oxide added concentration of 0.005 wt% and progressing to 0.330 wt%. At 0.005 wt% added sodium oxide in Solar Salt, the overall oxide ions concentration in the salt remains below the detection limit (<0.01 mol%) at t = 0. However, over time, the concentration gradually increases, reaching a final value of 0.062 mol% at 168 h. At 0.070 wt% added sodium oxide, the initial concentration is 0.062 mol% and increases to 0.112 mol% at 168 h. For 0.135 wt% added sodium oxide, the initial oxide ions concentration is 0.153 mol% and rises to 0.195 mol%. At 0.200 wt% added sodium oxide, the concentration starts at 0.255 mol% and increases to 0.262 mol%. For 0.265 wt% added sodium oxide, the concentration starts at 0.277 mol% and remains steady at 0.272 mol% at 168 h. Finally, at 0.330 wt% sodium oxide, the concentration starts at 0.375 mol% and remains steady around 0.348 mol%. Similar to sodium peroxide added Solar Salt, at low added sodium oxide concentration of 0.005 wt%, 0.070 wt%, and 0.135 wt%, the overall oxide ions concentration in the salt increases over time and do not appear to reach a steady-state. However, the addition of 0.200 wt%, 0.265 wt%, and 0.330 wt% sodium oxide results in a smaller increase in the overall concentration of oxide ions in the salt compared to the lower concentrations. Notably, the 0.265 wt% and 0.330 wt% sodium oxide concentrations exhibit also a quasi-steady-state behavior with no increase in oxide ions concentration over time. This behavior is similar to what was observed in sodium peroxide-added Solar Salt.

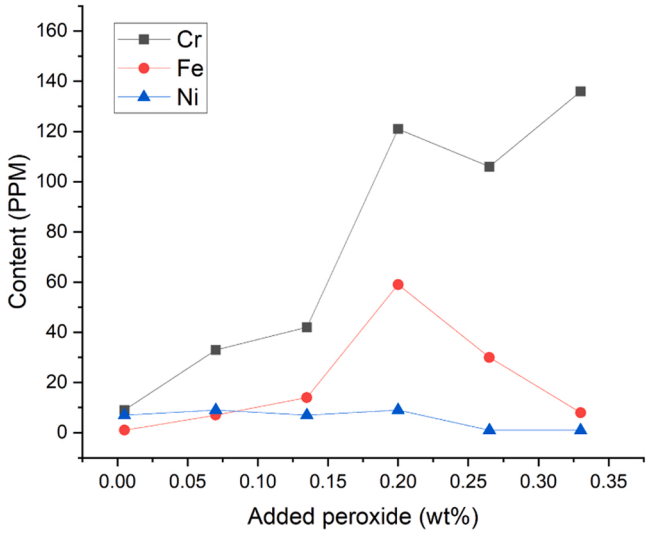

Fig. 4. Concentration of cations (Fe, Cr, and Ni) in Solar Salt with increasing sodium peroxide concentration determined by MP-AES after 168 h.

The nitrate and nitrite ion content measured for the reference samples through IC are shown in Fig. 5(b). At t = 168 h, the nitrate/nitrite content for sodium oxide impurity additions of 0.005 wt%, 0.070 wt%, 0.135 wt%, 0.200 wt%, 0.265 wt%, and 0.330 wt% reached the following values: 89.0/10.9 mol%, 89.5/10.4 mol%, 89.0/10.8 mol%, 89.9/9.9 mol%, 89.7/10.0 mol%, and 89.8/9.8 mol%, respectively. Regardless of the added sodium oxide impurity, the nitrate/nitrite content stabilizes around 89.5/10.3 mol% at 168 h. This observation is consistent with previously reported data with sodium peroxide added Solar Salt.

3.1.4. Sodium oxide impact on salt chemistry with steel

To analyze the impact of steel on sodium oxide added to Solar Salt, this subsection is specifically dedicated to discussing the evolution of salt chemistry with steel. First, the concentration of oxide ions measured through titration in the salt samples containing steel is discussed. Finally, the evolution of nitrate and nitrite ions are examined.

The change in oxide ions concentration over time is depicted in Fig. 5 (a), with filled symbols indicating the oxide ions concentration of steel containing salt samples. At 0.005 wt% added sodium oxide, the overall oxide ions concentration in the salt remains below the detection limit (<0.01 mol%) at t = 0. However, over time, the concentration gradually increases, reaching 0.079 mol% at 168 h. At 0.070 wt% added sodium oxide impurity, the initial concentration is 0.080 mol% and increases to 0.133 mol% at 168 h. For 0.135 wt% added sodium oxide impurity, the initial oxide ions concentration in the salt is 0.173 mol% and increases to 0.197 mol% at 168 h. For 0.200 wt% added sodium oxide, this value slightly increases from 0.262 mol% at t = 0–0.268 mol% at 168 h. For 0.265 wt% added sodium oxide, the concentration increases from 0.161 mol% at t = 0–0.208 mol% at 168 h. For 0.33 wt% added sodium oxide, the concentration decreases from 0.364 mol% at t = 0–0.264 mol % at 168 h. Moreover, for 0.265 wt% added sodium oxide, fluctuations in the measured oxide ion concentration are observed. This may be attributed to increased carbon dioxide absorption with rising oxide ion concentration in the salt, potentially leading to the observed variations [22] or accelerated consumption of these ions by steel to form other products. Comparing the evolution of oxide ions in the steel-containing salt with that of the reference salt, it is noteworthy that below the concentration of 0.135 wt% added sodium oxide ions, there was a slight increase in the overall concentration of oxide ions in the steel-containing salt samples compared to the reference salt samples. Above 0.135 wt% added sodium oxide, a slight decrease in oxide ions concentration is observed after 168 h compared to the reference salt samples. The variation in oxide ions concentration, with and without the presence of steel, suggests potential involvement of the steel or corrosion processes. A detailed discussion of these effects will be provided in the Section 4, following the analysis of the impact of added impurities on steel corrosion.

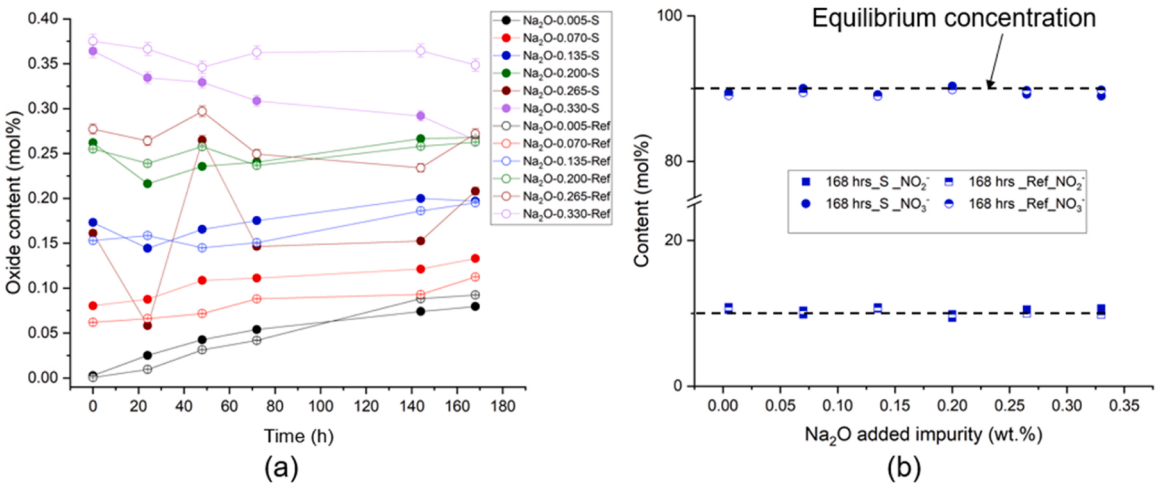

Fig. 5. Anion contents in Solar Salt at 600 °C with Na_2O added impurity a) Oxide ions concentration in Solar Salt measured from acid-base titration (error bars not visible are in the symbol size) b) Nitrate/nitrite content in Solar Salt measured through ion chromatography.

The nitrate and nitrite ion content measured for the steel containing Solar Salt samples through IC are shown in Fig. 5(b). Similar to the reference salt samples, at t = 168 h, the nitrate/nitrite content stabilizes around 89.5/10.3 mol% irrespective of the oxide addition. This indicates that after 168 h, the equilibrium between nitrate and nitrite in Solar Salt is not significantly influenced by the addition of sodium oxide, sodium peroxide, or the presence of steel. Instead, the equilibrium is primarily governed by the oxygen partial pressure over the salt, as described by Eq. 1.

Fig. 6 shows the change in metal (Fe, Cr, and Ni) concentration measured through MP-AES with increasing sodium oxide content in the Solar Salt. chromium (Cr) concentration increases from 28 PPM at 0.005 wt% to 207 PPM at 0.33 wt% with the addition of sodium oxide in Solar Salt. Similarly, iron (Fe) shows an increase from 2 PPM at 0.005 wt % to 285 PPM at 0.33 wt%. In contrast, nickel (Ni) impurities remain relatively low, with slight fluctuations ranging from 7 ppm at 0.005 wt% to 4 ppm at 0.33 wt%. As for Solar Salt with added peroxides, also added oxides showed high fluctuations in Fe concentration. They are attributed to the formation of corrosion products, which are not evenly distributed at higher concentrations of sodium oxide in the salt.

3.2. Steel analysis

3.2.1. Impact of sodium peroxide addition in the Solar Salt

In this subsection, results of the impact of added sodium peroxide impurity on the corrosion of AISI 316 L in Solar Salt are presented. First, the area-specific weight change after corrosion is presented, followed by the corrosion rate analysis. Additionally, the results from SEM-EDX, FIB, and GIXRD analyses are presented and discussed.

The area specific-weight change results are illustrated in Fig. 7(a). The area-specific weight change increases from 0.33 mg/cm² at 0.005 wt% sodium peroxide to 0.96 mg/cm² at 0.070 wt%. However, at 0.135 wt% sodium peroxide, the weight change decreases to 0.58 mg/cm², and further decreases to −3.38 mg/cm² at 0.200 wt%. Subsequent increases in sodium peroxide concentration to 0.265 wt% and 0.33 wt% lead to a significant decrease in weight, with values of −4.37 mg/cm² and −6.35 mg/cm², respectively. The initial increase in area-specific weight from 0.33 mg/cm² to 0.96 mg/cm² suggests an overall increase in the weight of the final samples after corrosion caused by oxide layer formation. However, the significant weight decrease observed after adding 0.135 wt% sodium peroxide suggests base metal loss. This metal loss is considered to be due to the formation of a non-adherent corrosion layer, which can lead to its spallation or detachment. The spallation can

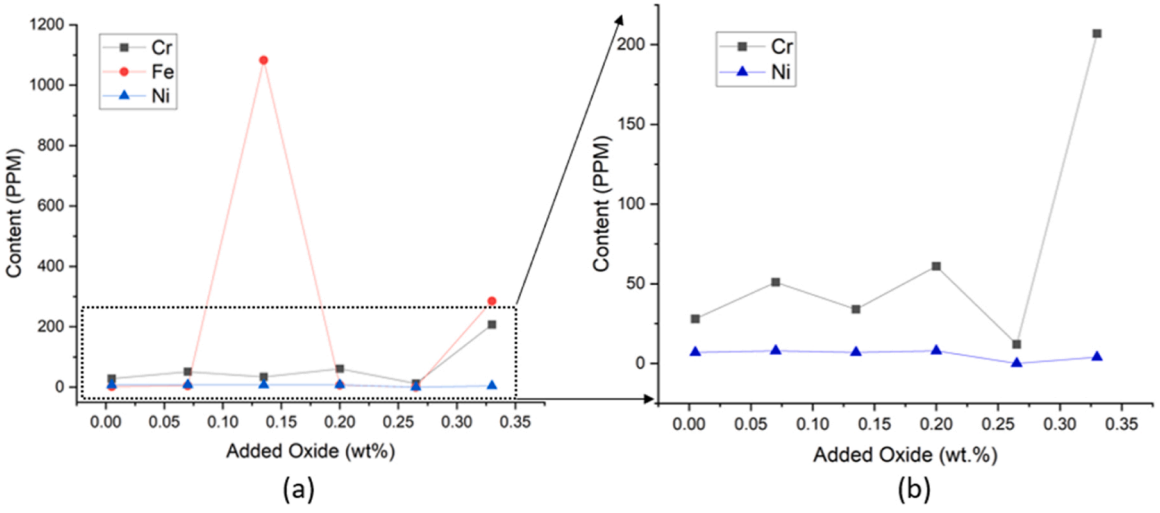

Fig. 6. (a) Concentration of cations (Fe, Cr, and Ni) with increasing sodium oxide concentration determined by MP-AES after 168 hrs at 600 °C in steel containing Solar Salt (b) Expanded view of the left graph's y-axis for Cr and Ni.

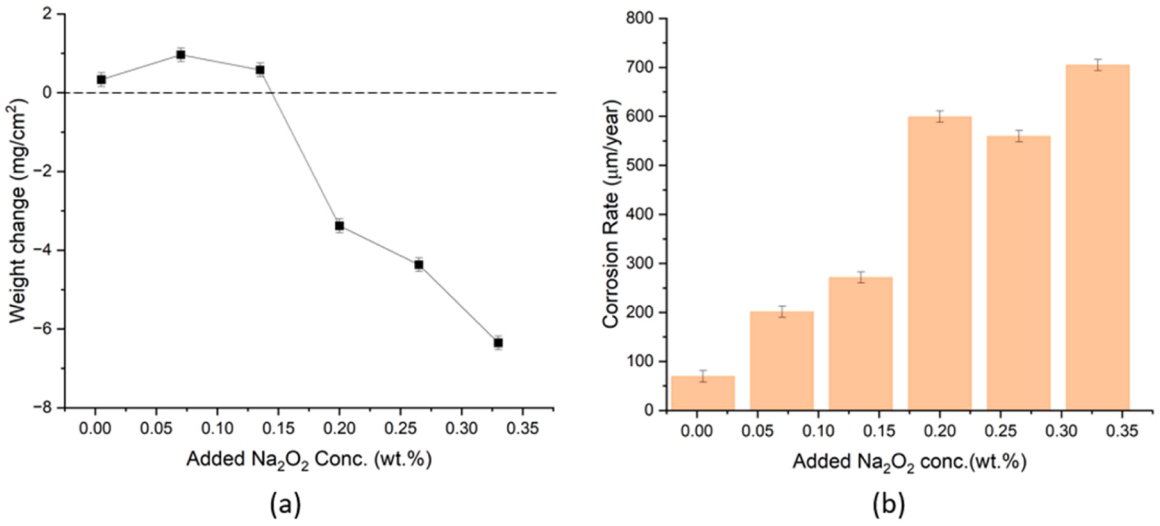

Fig. 7. (a) Area specific weight change, and (b) corrosion rate of AISI 316 L stainless steel estimated by descaled weight loss for added Na_2O_2 in Solar Salt, after 168 h of isothermal immersion at 600 °C.

occur due to the growth stress resulting from mismatch in the volume of formed corrosion layer and metal or thermally induced stresses arising from differences in coefficient of thermal expansion (CTE) [24].

To determine the amount of metal consumed during the corrosion process, descaling was performed on the final corroded samples. The corrosion rates were then calculated according to Eq. 5, with the corrosion rates for different sodium peroxide concentrations depicted in Fig. 7(b). The corrosion rate for 0.005 wt%, 0.070 wt%, 0.135 wt%, 0.200 wt%, 0.265 wt%, 0.33 wt% added sodium oxide is found to be 69 µm/year, 201 µm/year, 271 µm/year, 599 µm/year, 559 µm/year, and 704 µm/year respectively. The corrosion rate exhibits an increase up to 271 µm/year at 0.135 wt% added sodium peroxide. However, beyond this concentration, the corrosion rate rises significantly to 599 µm/year at 0.200 wt% added sodium peroxide, indicating a substantial amount of metal loss above 0.135 wt% added sodium peroxide. Overall, the area specific weight decreases significantly after the addition of 0.135 wt% sodium peroxide, while the corrosion rate increases notably once this concentration is exceeded. The two methods, therefore, show consistent results, which also indicate the high corrosivity of the salt above these concentrations.

To assess the impact of added sodium peroxide on the corrosion layer thickness and morphology, SEM-EDX analysis was conducted on samples with up to 0.20 wt% sodium peroxide. For samples with 0.265 and 0.33 wt% added sodium peroxide, where severe spallation was observed, the FIB cutting technique was employed to avoid damaging the top corrosion layer.

The SEM-EDX maps for sodium peroxide additions ranging from 0.005 wt% to 0.20 wt% and 0.265 wt% are shown in Figure A.1 and

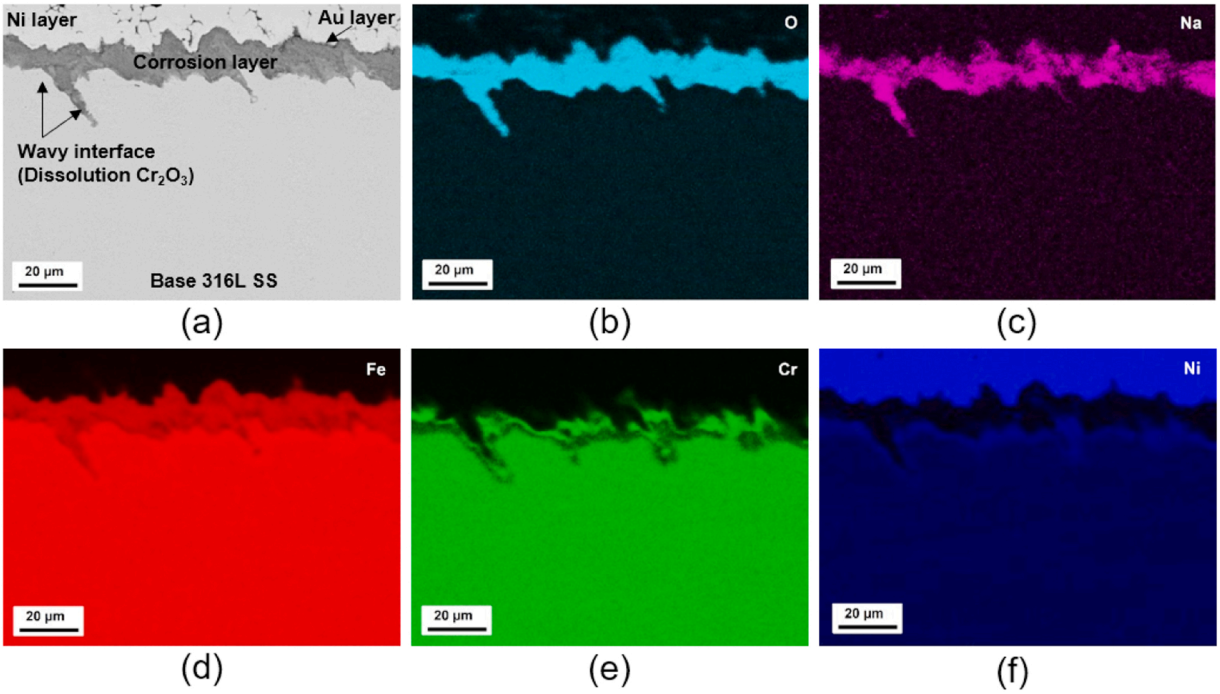

Fig. 8. (a) SEM-BSE cross-sectional morphology, and (b-f) the corresponding EDX elemental maps of the 316 L SS exposed with 0.005 wt% sodium peroxide added Solar Salt at 600 °C for 168 h in air.

Figure A.2, while the specific map for 0.005 wt% sodium peroxide concentration is presented in Fig. 8. Based on the elemental distribution map from SEM-EDX, the corrosion layers can be divided into four distinct zones. The first layer contains oxygen, sodium, and iron, indicating the formation of a sodium iron oxide ($NaFeO_2$) layer. Potassium seems to be present in negligible amount in the corrosion layer suggesting it is not a major component in the corrosion layer. This type of corrosion product is commonly observed in molten nitrate/nitrite molten salt corrosion at high temperatures [25–27]. Since this layer also exhibits sodium ion conduction, as studied in battery research [28], the movement of sodium ions through the iron oxide layer may compromises its passivating or protective abilities. Below the sodium iron oxide layer, an iron oxide layer can be observed, with traces of chromium indicating the formation of chromium-containing iron oxide. This layer is often associated with the spinel structure, which is commonly observed in corrosion products under high-temperature conditions for iron chromium alloys [29]. The innermost layer is enriched with chromium and oxygen, suggesting the formation of a chromium oxide (Cr_2O_3) layer, which is typically considered protective in nature due to its ability to form a stable, passive barrier against further corrosion. Just below the chromium oxide layer a chromium depletion and nickel enriched zone can be observed. As shown in Fig. 8, the 0.005 wt% added sodium peroxide, shows a different corrosion layer morphology, characterized by a wavy interface between the metal and the corrosion layer. Notably, similar to our earlier research with 0.005 wt% added sodium oxide [20], the addition of 0.005 wt% sodium peroxide also results in the formation of a wavy interface that contains no chromium. This absence is likely due to the well-documented solubility of the chromium oxide layer as chromate in nitrate salt [19,21]. It is possible that the presence of excess oxide ions contributes to a rapid basic dissolution of the chromium oxide layer, as explained by Rapp et al. through the fluxing mechanism [30].

Similar to the corrosion layer formation observed at lower concentrations of sodium peroxide, the corrosion layers formed at higher concentrations exhibit distinct layers (Fig. 9). Furthermore, cross-sectional analysis of corroded samples revealed that the corrosion layer thickness does not show a direct correlation with the overall corrosion rate. Instead, the thickness fluctuates with increasing oxide ion concentration, likely due to the dynamic balance between corrosion layer growth, dissolution, and spallation. The thickness of the corrosion layer does not exhibit a consistent increasing or decreasing trend with increasing sodium peroxide concentration, varying between 8.2 μm and 14.4 μm. This suggests that corrosion severity is not solely dictated by layer thickness but is also influenced by the stability and morphology of the oxide layers formed at different oxide ion concentrations. Interestingly, at higher concentrations of added sodium peroxide above 0.200 wt%, as illustrated in Fig. 9 for the sample with 0.33 wt% added sodium peroxide, porosity and defects begin to appear more in the sodium iron oxide corrosion layer, with a thin iron oxide layer. Additionally, disintegrated particles enriched with nickel and iron can be observed within a thick chromium oxide layer. Further discussion of this will be followed after the discussion of impact of sodium oxide on corrosion, in Section 5. To further analyse the structure and phases formed in the corrosion layer GIXRD was performed on all the steel samples exposed to sodium peroxide added solar salt.

Fig. 10 shows the GIXRD patterns as a function of the scattering vector Q, obtained from the AISI 316 L samples after exposing to Na_2O_2-added (0.005–0.33 wt%, in steps of 0.065 wt%) Solar Salt at 600 °C for 168 h. As stated in the experimental section, a diffractometer with Co X-ray source was used for the samples exposed to 0.005–0.20 wt% Na_2O_2-added Solar Salt whereas a diffractometer with Mo X-ray source was used for the samples exposed in 0.265 and 0.33 wt% conditions. The wavelength of a Co source is large which obviously shift the XRD patterns towards a larger Bragg angle, in contrast, a short wavelength of Mo source shifts the patterns towards a lower Bragg angle. Therefore, the scattering vector plot is presented here for a more straightforward

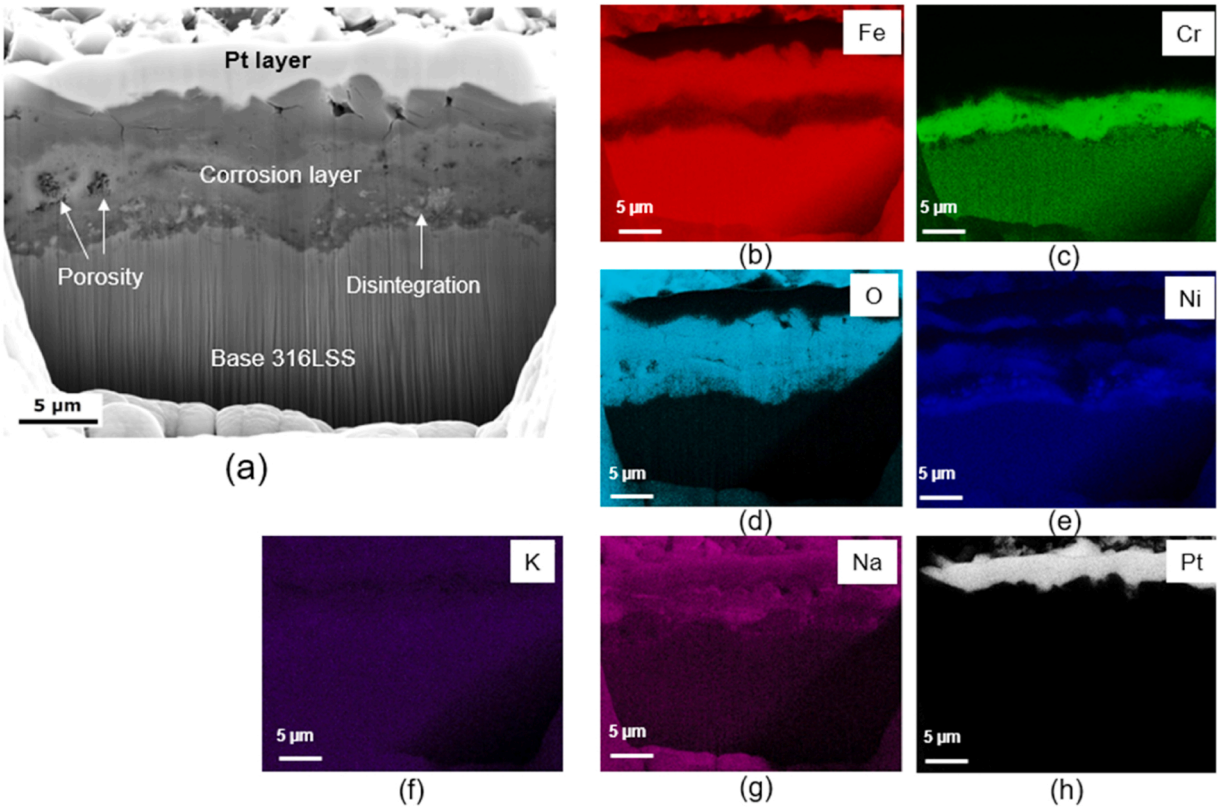

Fig. 9. (a) FIB cut cross-sectional morphology, and (b-h) the corresponding EDX elemental maps of the AISI 316 L with 0.33 wt% sodium peroxide added Solar Salt at 600 °C for 168 h in air.

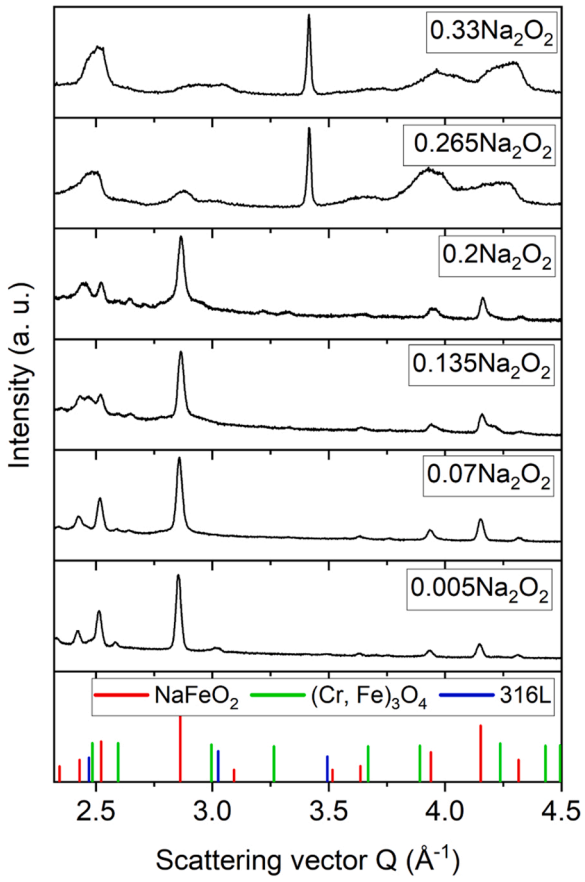

Fig. 10. The GIXRD patterns of AISI 316 L samples exposed to sodium peroxide added Solar Salt (at 600 °C for 168 h) plotted along scattering vector Q.

comparison analysis of the XRD patterns acquired from the different X-ray sources. In addition, for a better visual perception of differences and similarities of the oxide phases formed in the corrosion layer, the acquired patterns of all the samples exposed in Na_2O_2-added Solar Salt is displayed in the same plot, as illustrated in Fig. 10. Overall, the qualitative phase analysis, i.e., matching the measured diffraction patterns with the reference database indicates that the surface of the corrosion layer in all the Na_2O_2 peroxide exposed samples, is sodium ferrite ($NaFeO_2$), however, the obtained patterns of 0.265 and 0.33 Na_2O_2 samples, the surface coverage/distribution of $NaFeO_2$ may not be uniform. This means at higher concentration of peroxide addition into the molten nitrates, chemical homogeneity and/or compactness of the corrosion layer changes which can be evidenced by the apparent peak broadening at low Q-range. Additionally, the peak broadening may be attributed to increased sodium ingress into the formed $NaFeO_2$ layer, potentially leading to the formation of other non-stoichiometric compounds of $NaFeO_2$. In addition to the primary $NaFeO_2$ phase, a reflection at low Q-range around Q ~2.5 $Å^{-1}$ is attributed to the formation of spinel phases Fe_3O_4 and $(Cr, Fe)_3O_4$ and/or $(Cr, Ni, Fe)_3O_4$. The GIXRD results are consistent with the cross-sectional SEM-EDX and/or FIB-cut EDX observations. In 0.265 and 0.33 cases, a high intense narrow peak at Q ~3.4 $Å^{-1}$ is from the sample holder used in a diffractometer equipped Mo X-ray source and that was later found from the blank run, without sample (figure not shown here).

3.2.2. *Impact of sodium oxide addition in the Solar Salt*

In this subsection, the impact of the added sodium oxide impurity on the corrosion of AISI 316 L in Solar Salt is examined. First, the area specific weight change after corrosion is presented, followed by the corrosion rate results. Additionally, the results from SEM-EDX, FIB cross-sectioning, and GIXRD are presented and discussed.

The area specific weight change results are illustrated in Figure (a). The area-specific weight change increases from 0.35 mg/cm² at 0.005 wt% sodium oxide to 1.01 mg/cm² at 0.070 wt%. At 0.135 wt% sodium oxide, the weight change stabilizes at 0.92 mg/cm², but it decreases to −1.26 mg/cm² at 0.200 wt%. Further increases in sodium oxide concentration to 0.265 wt% and 0.33 wt% result in a significant decrease in weight change, with values of −11.23 mg/cm² and −9.77 mg/cm², respectively. The initial increase in the area specific weight change from 0.35 mg/cm² to 1.01 mg/cm², suggests the formation of corrosion products on the steel surface. Subsequently, the decrease in area-specific weight change from 0.92 mg/cm² to −9.77 mg/cm² indicates significant metal loss from the steel due to corrosion, with the formed corrosion products detaching from the steel surface. These results indicate that the losses are due to spallation.

The corrosion rate obtained from descaling is calculated as per Eq. 5. The corrosion rate for different added sodium oxide concentration is depicted in Figure (b). The corrosion rate for 0.005 wt%, 0.070 wt%, 0.135 wt%, 0.200 wt%, 0.265 wt%, 0.33 wt% added sodium oxide is found to be 173 μm/year,164 μm/year,198 μm/year, 275 μm/year, 916 μm/year, and 994 μm/year respectively. The corrosion rate exhibits a gradual increase, reaching 198 μm/year at 0.135 wt% added sodium oxide. However, beyond this concentration, the rate climbs further to 275 μm/year at 0.20 wt% added sodium oxide, indicating increased metal loss above 0.135 wt%. Additionally, beyond 0.20 wt%, the corrosion rate continues to rise significantly. Similar to the behavior observed in Solar Salt corrosion with added sodium peroxide, the area specific weight decreases significantly after the addition of 0.135 wt% sodium oxide. However, the corrosion rate increases notably once this concentration is surpassed. These trends suggest an excess of spallation and metal loss in the material beyond this concentration level in Solar Salt.

To analyze the impact of added sodium oxide on the cross-sectional morphology of steel samples, similar to the approach used for sodium peroxide described in the previous subsection 3.2.1, subsequent analysis of the corrosion layer was conducted to determine changes in corrosion thickness. SEM-EDX analysis were performed on samples with up to 0.20 wt% sodium peroxide. For samples with 0.265 and 0.33 wt% sodium oxide, where severe spallation was observed, the FIB cutting technique was employed.

The corrosion layers formed in sodium oxide-added Solar Salt exhibit similar characteristics compared to that of the corrosion layers formed in peroxide-added Soar Salt, as discussed in Section 3.2.1. As shown in Figure A.3, these layers consist of a top sodium iron oxide layer, followed by a chromium-containing iron oxide layer, then a chromium oxide layer, and finally, a nickel segregation or chromium depletion zone. The formation of the corrosion layer up to 0.20 wt% added sodium oxide in Solar Salt has already been discussed in detail in our earlier research [20]. It was found that when the sodium oxide concentration exceeded 0.135 wt%, the corrosion layer's disintegration increased. The threshold for corrosion layer disintegration in sodium oxide-added Solar Salt was identified at 0.135 wt%, where significant degradation and porosity in the corrosion layer were observed. Similar to earlier observations for sodium peroxide, when the concentration of sodium oxide exceeds 0.20 wt%, the corrosion layer exhibits a disintegrated structure. This is shown in Fig. 12 for 0.265 wt% added sodium oxide. The top corrosion layer, composed of sodium iron oxide, shows significant disintegration, with vertical and horizontal cracks becoming more prominent. Beneath this layer, a highly porous iron oxide layer is observed, along with a thick chromium oxide layer, indicating severe degradation of the protective oxide structure. Moreover, as shown in Figure A.4, the top sodium iron oxide layer can also detach, leading to a thinner corrosion layer. This explains why the overall corrosion layer thickness does not exhibit a consistent increase or decrease with increasing sodium oxide concentration, instead varying between 3.8 μm and 16.9 μm, similar to the observations for sodium peroxide-added

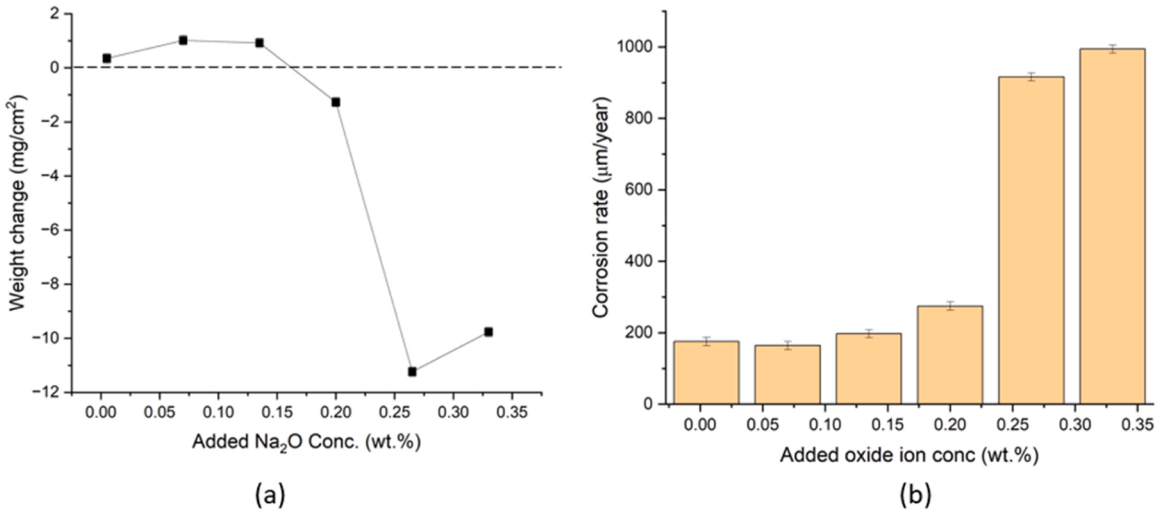

Fig. 11. (a) Area specific weight change (error bars not visible are in the symbol size) (b) Descaling mass loss for added sodium oxide impurity in Solar Salt at 600 °C after 168 h (7 days) of corrosion test.

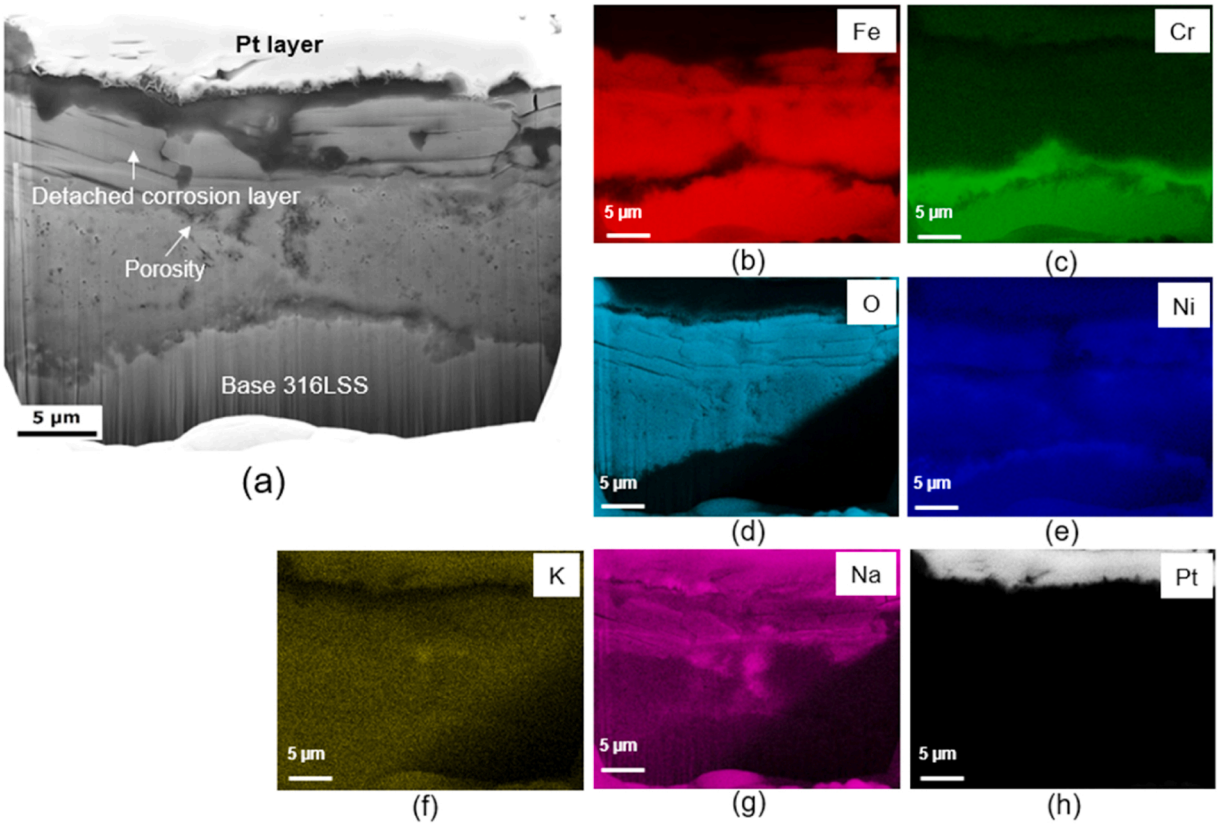

Fig. 12. (a) FIB cut cross-sectional morphology, and (b-h) the corresponding EDX elemental maps of the AISI 316 L SS exposed to 0.265 wt% of sodium oxide added Solar Salt at 600 °C for 168 h in air.

Solar Salt. To further analyze the structure and phases of the corrosion layer, GIXRD was performed.

The scattering vector plot obtained through the GIXRD patterns acquired from the AISI 316 L samples exposed to Na_2O-added (0.005–0.33 wt%, in steps of 0.065 wt%) Solar Salt at 600°C for 168 h is shown in Fig. 13. Assigned diffraction peaks clearly illustrating that the sodium ferrite ($NaFeO_2$) phase exist as a dominant phase at the outermost corrosion layer. The large difference appears above 0.07 wt% added sodium oxide where the doublet regime of $NaFeO_2$ phase in low Q-range appears to broaden with the emergence of new tiny peaks that attributes to the presence of Fe_3O_4 and/or (Cr, Fe)$_3O_4$ mixed oxide spinel phase. It must be noted that difference in high intense peaks of $NaFeO_2$ in scattering vector plot is expected which is basically due to the difference in wavelengths of the diffractometers. At 0.33 wt% added sodium oxide, the peak's intensity pattern as well as their number increase with broadening indicates the existence of γ-Fe phase in addition to the characteristics $NaFeO_2$ and spinel phases (Cr, Fe) $_3O_4$/ (Cr, Ni, Fe)$_3O_4$ and/or Fe_3O_4. More strikingly, the emergence of steel matrix

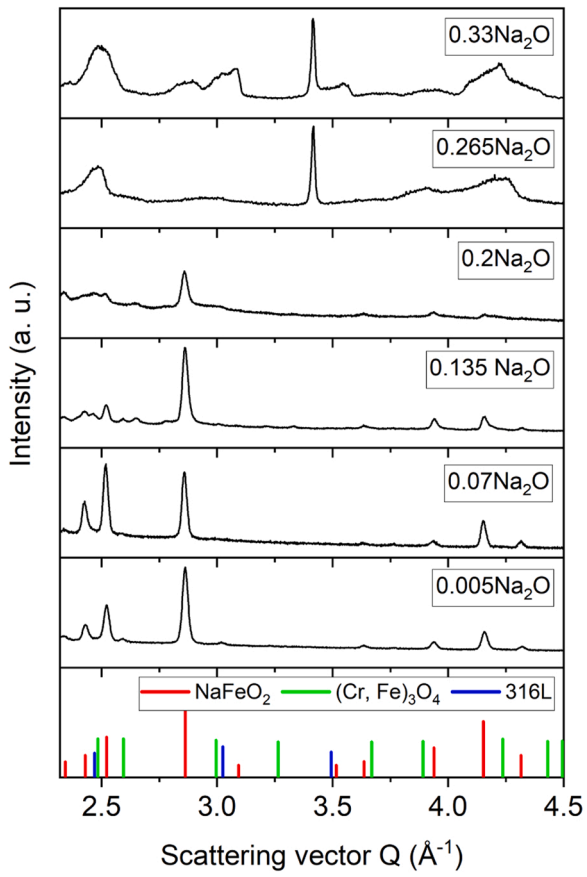

Fig. 13. The GIXRD patterns of 316 L SS samples exposed to sodium oxide (Na_2O)-added Solar Salt (at 600 °C for 168 h) plotted along scattering vector Q.

phase evidencing that the corrosion layer is thin for higher concentration (>0.265 wt%) of added sodium oxide, which concludes occurrence of severe spallation. This is also further evidenced by cross-sectional examination of the corrosion layer formed in 0.265 wt% Na_2O (see FIB-cut and the corresponding EDX elemental maps in Fig. 12). The observed broadness in peak's feature with increase of Na_2O concentration, in particular, ≥ 0.135 wt% Na_2O is most likely a consequence of difference in oxide crystallite size of multiphase mixture within the corrosion layer. By combining the phases found through GIXRD results and the cross-sectional examination of the corrosion layers by SEM-EDX and/or FIB-EDX give valuable information about the corrosion conditions and reactions influenced by the addition of oxide/peroxide impurities into the Solar Salt.

4. Discussion

Overall, the steel analysis reveals significant changes in the corrosion behavior due to the addition of sodium oxide or peroxide impurities in the Solar Salt mixture. Beyond 0.135 wt% of added oxide or peroxide, the area-specific weight change becomes negative, indicating severe spallation or detachment of the corrosion layer. Furthermore, the significant increase in corrosion rate above 0.20 wt% of added sodium oxide or peroxide impurities indicates a higher metal loss or consumption rate above this oxide impurity threshold. It is important to note that the overall thickness of the corrosion layer in Solar Salt with added sodium oxide or peroxide, as measured by SEM (Figure A.1 and A.3), does not follow a consistent trend with increasing sodium oxide or peroxide concentration, fluctuating between 8 μm and 14 μm. This inconsistency in thickness can also be also attributed to the spallation of the formed corrosion layer, which is linked to the defects and porosity within it, leading to detachment. These defects and porosity in the corrosion layer are supported by FIB cut results (Figs. 9 and 12) and MP-AES data (Figs. 4 and 6), which show increased metal content in the salt after 0.135 wt% added concentration.

Correlating these results with the salt chemistry shows that oxide ions start to decrease more significantly above 0.135 wt% of added sodium oxide or peroxide when the steel is present in the salt, compared to when the steel is not present (Figs. 3(a) and 5(a)). This observation also indicates a consumption or active participation of the added sodium oxide and peroxide in the corrosion process. However, the specific type of oxide ions present in the nitrate salt are not fully understood. The detection method used in our study, namely titration, measures the total oxide ion concentration, which includes contributions from all oxide species and does not differentiate among the different oxide ion species. However, some of the literature suggest that oxides, peroxide and superoxide are in equilibrium with the nitrate and nitrite ions as per the following Equation and can convert to one another based on the oxygen transfer reaction Eqs. 6 and 7 [9,23,31].

$$O^{2-} + NO_3^- \rightleftarrows O_2^{2-} + NO_2^- \quad (6)$$

$$O_2^{2-} + 2NO_3^- \rightleftarrows 2NO_2^- + 2O_2^- \quad (7)$$

It could be possible that the added sodium oxide and peroxide impurity can convert to one another in the nitrate melt first and then participate in the corrosion process. This may explain the similar behavior of both added sodium oxide and sodium peroxide on salt chemistry and steel corrosion, as the exact types of oxide ions present are not fully known. For further discussion, the term "oxide ions" will be used to describe the corrosion process.

Oxide ions are known to increase the basicity of any salt melt, as described by the Lux-Flood acid-base theory for oxide melts[32]. In the following section, the changes in the three distinct corrosion layers formed on the steel surface are discussed, along with the effects of higher levels of oxide ions / higher basicity of the melt. The analysis begins with the impact of increased oxide ions or basicity on the formation of the top sodium iron oxide layer, followed by a discussion of the middle iron oxide layer, and finally the chromium oxide layer.

The top corrosion layer is primarily composed of sodium, iron, and oxygen. As the oxide ions concentration increases up to 0.33 wt%, the top layer remains similar in terms of their elemental constituents, namely sodium, iron, and oxygen. Earlier research has shown that the direct interaction of nitrate or nitrite ions can oxidize iron on the surface, forming iron oxide as per Eqs. 8 or 9. Additionally, sodium ions can be incorporated into the iron oxide layer through diffusion to form sodium iron oxide layer [33–35].

$$Fe + NO_3^- \rightleftarrows FeO + NO_2^- \quad (8)$$

$$3Fe + 3NO_3^- \rightleftarrows Fe_3O_4 + NO_2^- + 2NO + O^{2-} \quad (9)$$

However, when the concentration of added oxide ions exceeds 0.20 wt%, the integrity of the formed sodium iron oxide layer begins to change. Further additions of oxide ions in the salt resulted in porosity and cracks within the sodium iron oxide corrosion layer. This can be attributed to the enhanced kinetics of the corrosion layer formation. As studied by Furukawa et al., sodium oxide or sodium peroxide can oxidize the iron on the surface in contact, resulting in the formation of various sodium iron oxides, as demonstrated by the reaction in Eq. 10. Additionally, different forms of $NaFeO_2$ may also be produced depending on the sodium ion activity [36].

$$Fe + Na_2O_2 + Na_2O \rightleftarrows Na_4FeO_3 \quad (10)$$

Moreover, earlier work on low carbon mild steel immersed in $NaNO_3$-NaCl salt melt by Singh et al. demonstrates that the formation of $NaFeO_2$ in moderate basic media whereas $Na_4Fe_2O_5$ in strong basic condition and simply Fe_2O_3 in acidic media [37]. Therefore, it can be postulated that salt basicity is a major influential factor on the formation

of exterior corrosion layer and the increase in defects and porosity is due to the kinetically favored formation of the $NaFeO_2$ top layer, where a faster formation rate may result in a defect-prone structure or increased sodium diffusion within the layer. Additionally, Bonk et al. also demonstrated that controlling oxide ions formation in Solar Salt using a nitrogen oxide purge gas can lower the formation rate of the $NaFeO_2$ layer, resulting in a dense, topotactic $NaFeO_2$ structure that helps reduce further corrosion from the salt [35]. Based on our findings and existing literature, it is evident that the structural integrity of the top sodium iron oxide layer plays a crucial role in mitigating corrosion in molten Solar Salt. The key factor in maintaining this integrity is the oxide ions concentration in the salt, which directly influences the corrosion process.

Furthermore, the increase in defects and porosity within the sodium iron oxide layer can lead to direct interaction or diffusion of molten salt with the underlying iron oxide layer. Since the compromised top layer becomes less effective at protecting the inner layer, sodium and oxide ions can penetrate more deeper into the corrosion layer. In Figs. 9 and 12 showing cross sections for a high oxide ions concentration in the salt, a very thin iron oxide corrosion layer is evident. GIXRD analysis (Figs. 10 and 13) further confirms this, showing that the porous layer is characterized by broadened peaks, with reflections from the base metal becoming increasingly apparent above 0.20 wt% added impurity. It is possible that the iron oxide formed during the initial corrosion process can transform into a sodium iron oxide layer in presence of excess sodium oxide ions. This phenomenon is further supported by other researchers, who demonstrated that in the presence of an oxidizing nitrate salt (containing sodium nitrate), the conversion of iron oxide to sodium iron oxide occurs at a significantly faster rate compared to normal molten nitrates, as shown in Eq. 11 [28,38]. Therefore, the presence of oxide ions in the Solar Salt can lead to a thinner iron oxide layer.

$$Fe_2O_3 + Na_2O \rightleftarrows 2NaFeO_2 \quad (11)$$

Compared to the top corrosion layer of sodium iron oxide and iron oxide, the chromium oxide layer shows a less dense and thicker structure for increasing oxide concentrations. Typically, the chromium oxide layer is known to be protective in nature in high temperature gaseous environments, in contrast, chromium is highly soluble in nitrate molten salt as chromate [13]. Further addition of oxide ions in the melt can accelerate the dissolution of the chromium oxide layer into chromate, as confirmed by MP-AES data, which show an increase in chromium concentration with higher oxide content (Figs. 4 and 6). The dissolution of chromium from steel in oxide-ion-rich melts has been extensively studied for sulfate melts. Zhang et al. also proposed that in a basic melt the direct interaction of oxide ions with chromium oxide can lead to the formation of chromate ions [39]. This process can be represented by Eq. 12 using sodium as example cation.

$$Cr_2O_3 + 2Na_2O + \frac{3}{2}O_2 \rightleftarrows 2Na_2CrO_4 \quad (12)$$

The increased dissolution of chromium oxide as chromate can lead to faster outward diffusion or flux of chromium to the corroding steel surface, where it forms chromium oxide. Additionally, the rapid basic dissolution of chromium oxide to chromate in the basic molten salt results in a dispersed and thick chromium oxide layer, as observed in Figs. 9 and 12. Moreover, the nickel concentration in the melt was found to be relatively consistent according to the MP-AES data. This suggests that nickel is not highly soluble in the melt at oxide levels up to 0.33 wt %. However, nickel can diffuse into the corrosion layer, forming nickel oxide or remaining as a nickel layer just below the chromium oxide layer, without significantly participating in the corrosion reaction.

Based on the discussion regarding the formation of corrosion layer with different levels of added oxide concentration, the corrosion process can be summarized and divided into two parts, as illustrated in Fig. 14. At low oxide ion concentrations below 0.135 wt%, a thick and less porous $NaFeO_2$ layer (1) forms due to the relatively slow kinetics of formation, which results from the slower metal oxidation process driven by the oxide ions present in the salt. This slower formation rate prevents the corrosive salt from easily penetrating the iron oxide layer (2), allowing the iron oxide to grow thicker. The chromium dissolution through the iron oxide layer is also limited due to the denser and thicker nature of the iron oxide layer, which effectively supports the chromium oxide layer (3) and preserves its passivating properties. As a result, further corrosion is inhibited. Beneath the chromium oxide layer, a chromium depletion and nickel segregation zone (4) develops, though it does not significantly contribute to the corrosion process. Overall, the slower oxidation rate and reduced corrosion at low oxide ion concentrations below 0.135 wt% contribute to the formation of passivating and protective corrosion layers.

In contrast, at high oxide ion concentrations above 0.20 wt%, a thicker and more porous $NaFeO_2$ layer (1) forms due to increased metal oxidation and accelerated kinetics of layer formation. The increased

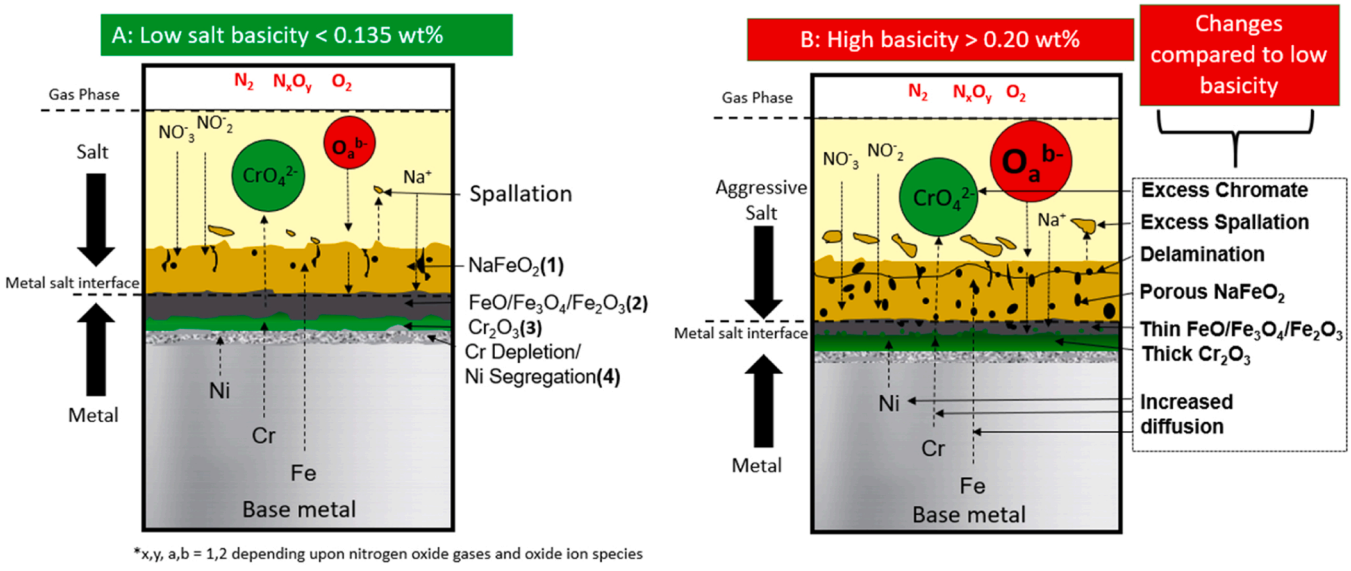

Fig. 14. Schematic representation of corrosion mechanisms in stainless steel (here AISI 316 L) exposed to Solar Salt with two basicity levels at 600 °C. (A) Low salt basicity (< 0.135 wt%): The salt exhibits a relatively stable interface with limited spallation (B) High basicity (> 0.20 wt%): Increased salt aggressiveness leads to excessive spallation, delamination, and the formation of porous corrosion products.

porosity and fragile nature of the corrosion layer can lead to spallation, causing it to detach from the steel surface. In the absence of a denser top corrosion layer, the iron oxide layer (2) begins to oxidize to $NaFeO_2$, resulting in a reduction of few microns in the thickness of the iron oxide layer. A thin and disintegrated iron oxide layer can also accelerate the dissolution of chromium oxide (3) through this layer, leading to the formation of chromate in the Solar Salt. This can result in excessive diffusion of chromium to the surface, forming a less dense and thicker chromium oxide layer that lacks protective capabilities, thereby promoting further corrosion of the base metal. While the exact initiation point of corrosion layer disintegration cannot be precisely determined using SEM-EDX, the results from weight change, corrosion rate, and GIXRD indicate that at oxide ion concentrations above 0.20 wt%, the corrosivity of the salt significantly increases for stainless steel at 600 °C. This knowledge is crucial for CSP-TES systems, as normal Solar Salt in an air atmosphere can exhibit rising oxide ion concentrations. If not controlled to a maximum level of 0.20 wt% or 0.25 mol% (oxide anion mol%), this can lead to significant damage to structural materials and potential future failure. It is suggested to focus on refining the monitoring and control mechanisms for oxide ion concentrations to mitigate corrosion risks of plants effectively. Ultimately, understanding these critical thresholds allows for better materials selection and corrosion management strategies, ensuring the longevity and efficiency of CSP-TES systems in operational environments.

5. Conclusion

This study explored the impact of adding up to 0.33 wt% sodium peroxide or sodium oxide to the Solar Salt at 600 °C for 168 h in synthetic air. Both salt and steel were analyzed to understand the corrosion mechanism and the role of oxide ions. Salt analysis was conducted using IC, titration, and MP-AES for nitrate/nitrite ions, oxide ions, and metal species, respectively. Steel corrosion was examined via weight change measurement, mass loss by descaling, SEM-EDX, FIB and XRD. This led to the following conclusions:

- **Impact of added impurities on Solar Salt:** Without the presence of stainless steel in Solar Salt, the impact of added sodium oxide and sodium peroxide shows a similar pattern in altering the oxide ions present in Solar Salt. Below 0.135 wt%, there is an increasing oxide ions trend with time, while above this concentration, a relatively steady concentration is observed, indicating the establishment of a quasi-steady-state equilibrium of oxide ions. The similar behavior of sodium oxide and sodium peroxide suggest that a conversion of one oxide ion type into the another could likely occur.

- **Nitrate and nitrite involvement in corrosion:** Nitrate and nitrite ions reach equilibrium concentration at 168 h, indicating that, in the long term, the addition of oxide impurities does not influence the nitrate and nitrite equilibrium. This equilibrium also remains unaffected by the presence of these impurities or steel.
- **Impact of steel on oxide ions:** The overall decrease in the concentration of oxide ions measured through titration when steel is present, compared to when steel is absent above 0.135 wt%, signifies a direct involvement of oxide ions in the corrosion process.
- **Impact of oxide ions on steel:** In the presence of steel, the concentration of metallic ions in the salt tends to increase above 0.135 wt% of added sodium oxide or peroxide. Moreover, beyond this concentration, the addition of sodium oxide or peroxide results in negative weight change, higher corrosion rates, and the formation of a porous and disintegrated corrosion layer. These findings suggest an intensifying molten salt attack on the steel at impurity levels exceeding 0.135 wt%.
- **Change in Corrosion Layer Morphology:** The structural integrity and porosity of the corrosion layer undergo significant changes beyond the critical concentration of 0.135 wt% of added oxide Na_2O or Na_2O_2 to the solar salt. Specifically, the $NaFeO_2$ layer becomes porous, crack-prone, and less protective. This is followed with the formation of a thin iron oxide layer, and finally a less dense, porous, and disintegrated chromium oxide layer. These observations highlight the impact of increased oxide ion concentrations on the corrosion behavior of steel.
- **Critical oxide ions concentration:** Elevating the oxide ions concentration, regardless of sodium oxide or sodium peroxide addition, to around 0.135–0.20 wt% and above correlates with an increase in the corrosivity of the salt at 600 °C, suggesting that this concentration represents a critical threshold for these ions in Solar Salt for stainless steel.

To summarize, this work highlights the critical role of oxide ions in Solar Salt corrosion, showing for the first time that these ions directly participate in the corrosion process, significantly altering salt corrosivity at 600 °C for austenitic stainless steel 316 L. This study also underscores the importance of controlling oxide ions to ensure the longevity of CSP-TES systems. Future research should explore the effects of increased oxide ion concentrations on mechanical and thermal stresses in molten salt storage tanks and other system components.

CRediT authorship contribution statement

Bauer Thomas: Writing – review & editing, Validation, Supervision, Resources, Project administration, Formal analysis. **Kumar Sumit:** Writing – review & editing, Writing – original draft, Visualization, Validation, Project administration, Methodology, Investigation, Formal analysis, Data curation, Conceptualization. **Swaminathan Srinivasan:** Conceptualization, Writing – review & editing, Writing – original draft, Visualization, Project administration, Methodology, Investigation, Formal analysis, Data curation. **Ding Wenjin:** Writing – review & editing, Supervision, Formal analysis. **Bonk Alexander:** Writing – review & editing, Supervision, Methodology, Conceptualization. **Hesse Rene:** Investigation, Data curation. **Goldbeck Hennig:** Investigation, Data curation.

Declaration of Competing Interest

The authors declare that they have no known competing financial interests or personal relationships that could have appeared to influence the work reported in this paper.

Acknowledgements

This work was supported by the Deutsche Forschungsgemeinschaft (DFG) – the German Research Foundation – through the funding (project number: 455432503) for the project 'Materials Degradation Phenomena of High Temperature Alloys by Molten Salts (MaDMoS).' The authors gratefully acknowledge M. Braun, R. Hoffmann, and A. Hanke for their assistance in the laboratories, and special thanks to Dr. A. Fantin at BAM for facilitating this work with the qualitative phase analysis using TOPAS software.

Appendices

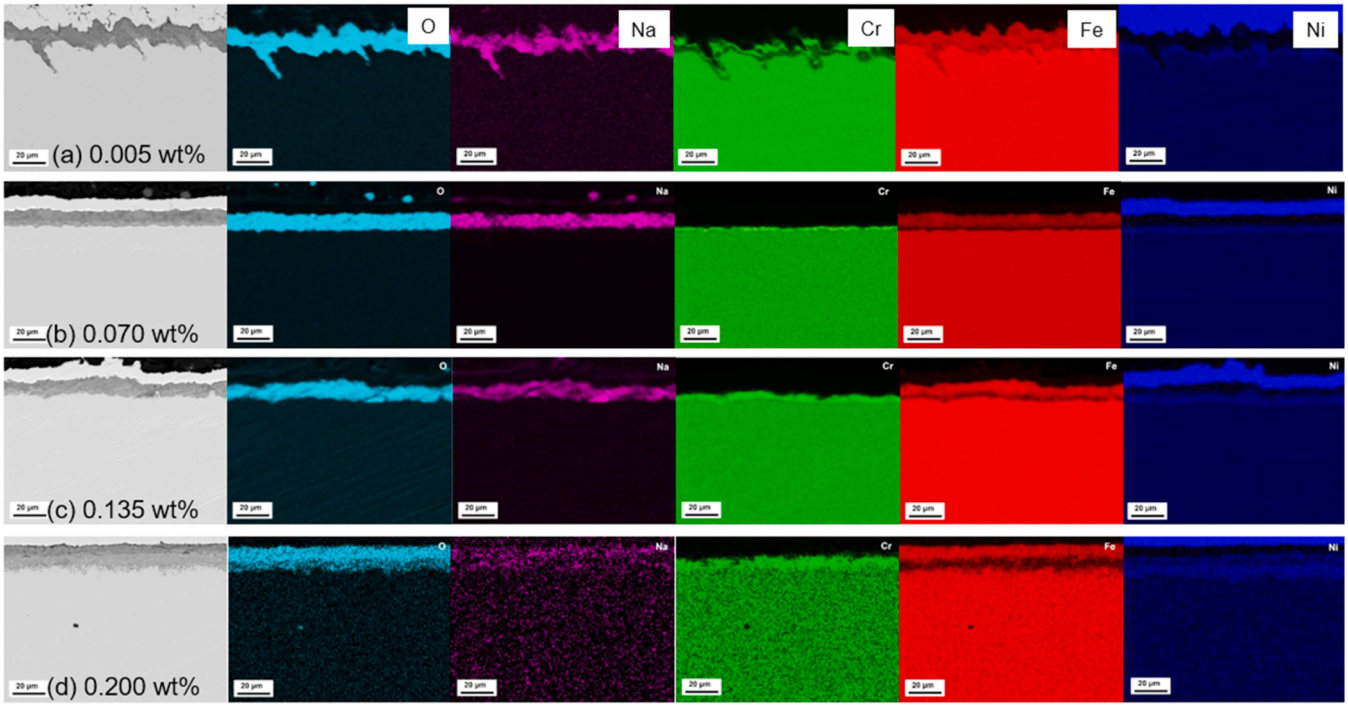

A.1. SEM cross-sectional images and corresponding elemental EDX maps of AISI 316 L after exposed to Solar Salt with sodium peroxide concentrations of (a) 0.005 wt%, (b) 0.070 wt%, (c) 0.135 wt%, and (d) 0.200 wt% at 600°C for 168 h in air

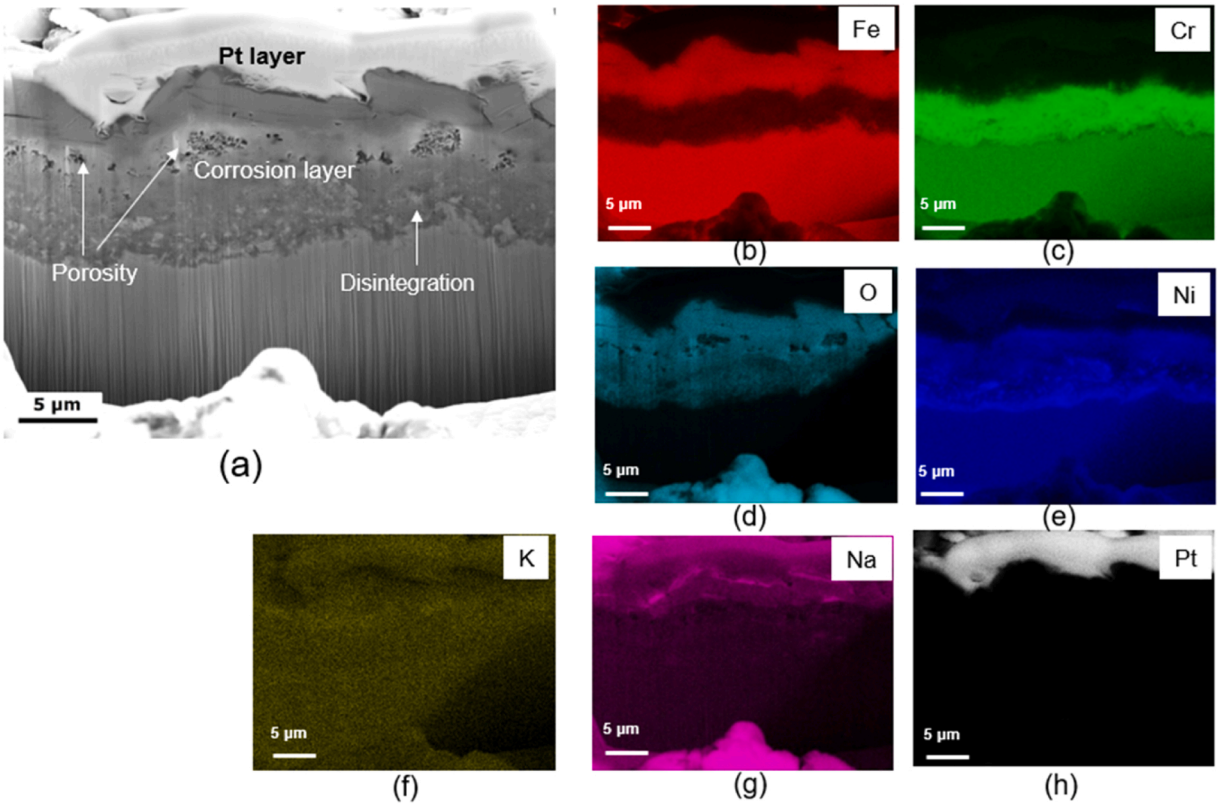

A.2. (a) FIB cut cross-sectional morphology, and (b-g) the corresponding EDX elemental maps of the AISI 316 L SS exposed to 0.265 wt% of sodium peroxide added Solar Salt at 600 °C for 168 h in air

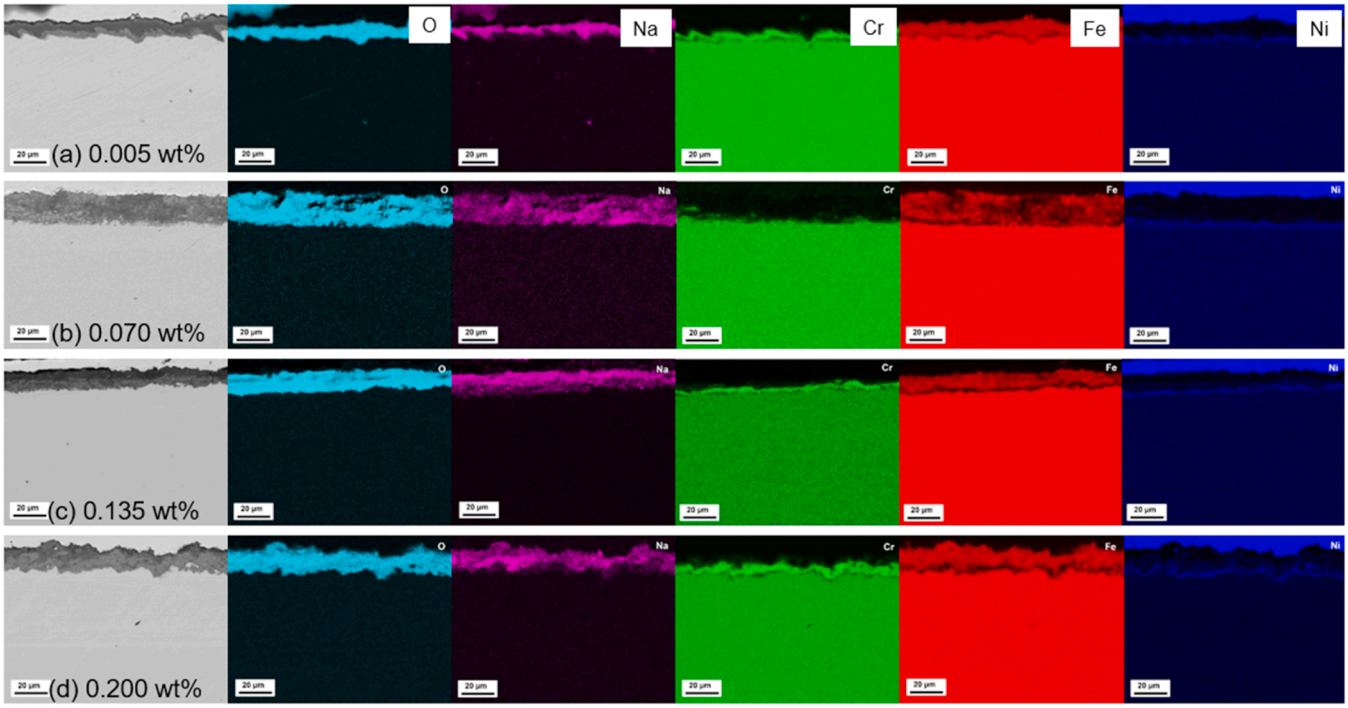

A.3. SEM cross-sectional images and corresponding elemental EDX maps of AISI 316 L after exposed to the Solar Salt with sodium oxide concentrations of (a) 0.005 wt%, (b) 0.070 wt%, (c) 0.135 wt%, and (d) 0.200 wt% at 600°C for 168 h in air

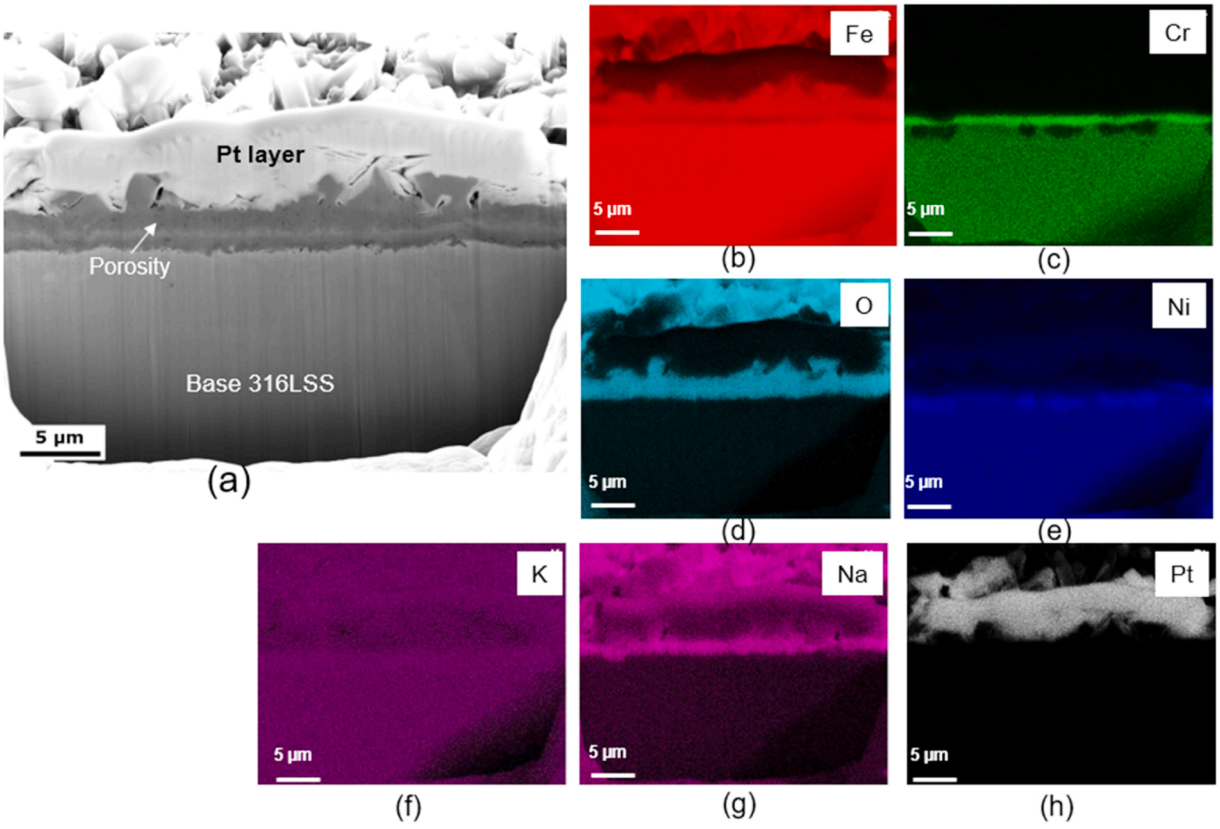

A.4. (a) FIB cut cross-sectional morphology, and (b-h) the corresponding EDX elemental maps of the AISI 316 L SS exposed to 0.330 wt% of sodium oxide added Solar Salt at 600 °C for 168 h in air

Data availability

Data will be made available on request.

References

[1] O. Achkari, A. El Fadar, Latest developments on TES and CSP technologies–Energy and environmental issues, applications and research trends, Appl. Therm. Eng. 167 (2020) 114806, https://doi.org/10.1016/j.applthermaleng.2019.114806.

[2] T. Bauer, C. Odenthal, A. Bonk, Molten salt storage for power generation, Chem. Ing. Tech. 93 (2021) 534–546, https://doi.org/10.1002/cite.202000137.

[3] D.A. Nissen, D.E. Meeker, Nitrate/nitrite chemistry in NaNO3-KNO3 melts, Inorg. Chem. 22 (1983) 716–721, https://doi.org/10.1021/ic00147a004.

[4] E.S. Freeman, The kinetics of the thermal decomposition of potassium nitrate and of the reaction between potassium nitrite and oxygen, J. Am. Chem. Soc. 79 (1957) 838–842, https://doi.org/10.1039/J19660001265.

[5] V.A. Sötz, A. Bonk, J. Forstner, T. Bauer, Microkinetics of the reaction NO3-⇌ NO2- + 0.5 O2 in molten sodium nitrate and potassium nitrate salt, Thermochim. Acta 678 (2019) 178301, https://doi.org/10.1016/j.tca.2019.178301.

[6] R.F. Bartholomew, A study of the equilibrium KNO3 (l)⇄ KNO2 (l)+ 1/2O2 (g) over the temperature range 550-750, J. Phys. Chem. 70 (1966) 3442–3446, https://doi.org/10.1021/j100883a012.

[7] R.I. Olivares, The thermal stability of molten nitrite/nitrates salt for solar thermal energy storage in different atmospheres, Sol. Energy 86 (2012) 2576–2583, https://doi.org/10.1016/j.solener.2012.05.025.

[8] V.A. Sötz, A. Bonk, J. Steinbrecher, T. Bauer, Defined purge gas composition stabilizes molten nitrate salt-Experimental prove and thermodynamic calculations, Sol. Energy 211 (2020) 453–462, https://doi.org/10.1039/J19660001265.

[9] P.G. Zambonin, J. Jordan, Redox chemistry of the system O2-O2–O22–O2-in fused salts, J. Am. Chem. Soc. 91 (1969) 2225–2228, https://doi.org/10.1021/ja01037a007.

[10] A. Bonk, M. Braun, V.A. Sötz, T. Bauer, Solar salt–pushing an old material for energy storage to a new limit, Appl. Energy 262 (2020) 114535, https://doi.org/10.1016/j.apenergy.2020.114535.

[11] J. Steinbrecher, A. Bonk, V.A. Sötz, T. Bauer, Investigation of regeneration mechanisms of aged solar salt, Materials 14 (2021) 5664, https://doi.org/10.3390/ma14195664.

[12] Á.G. Fernández, L.F. Cabeza, Molten salt corrosion mechanisms of nitrate based thermal energy storage materials for concentrated solar power plants: a review, Sol. Energy Mater. Sol. Cells 194 (2019) 160–165, https://doi.org/10.1016/j.solmat.2019.02.012.

[13] A. Bonk, D. Rückle, S. Kaesche, M. Braun, T. Bauer, Impact of Solar Salt aging on corrosion of martensitic and austenitic steel for concentrating solar power plants, Sol. Energy Mater. Sol. Cells 203 (2019) 110162, https://doi.org/10.1016/j.solmat.2019.110162.

[14] J. Slusser, J. Titcomb, M. Heffelfinger, B. Dunbobbin, Corrosion in molten nitrate-nitrite salts, JOM 37 (1985) 24–27, https://doi.org/10.1007/BF03259692.

[15] K. Federsel, J. Wortmann, M. Ladenberger, High-temperature and corrosion behavior of nitrate nitrite molten salt mixtures regarding their application in concentrating solar power plants, Energy Procedia 69 (2015) 618–625, https://doi.org/10.1016/j.egypro.2015.03.071.

[16] S. Marchiano, A. Arvia, Thermodynamics of iron/molten-sodium-nitrate, Electrochim. Acta 17 (1972) 25–32, https://doi.org/10.1016/0013-4686(72)85004-7.

[17] S.L. Marchiano, A.J. Arvia, Potential/pO2− diagrams of iron, cobalt and nickel in molten sodium nitrite, Electrochim. Acta 17 (1972) 861–871, https://doi.org/10.1016/0013-4686(72)90009-6.

[18] M.G. Fontana, N.D. Greene, Corrosion engineering, McGraw-hill, 2018.

[19] S. Kumar, A. Hanke, A. Bonk, T. Bauer, Influence of atmosphere and austenitic stainless steel on the solar salt corrosivity, Heliyon 10 (2024), https://doi.org/10.1016/j.heliyon.2024.e25966.

[20] S. Swaminathan, S. Kumar, A. Kranzmann, R. Hesse, H. Goldbeck, A. Fantin, Corrosion characteristics of 316L stainless steel in oxide-rich molten solar salt at 600° C, Sol. Energy Mater. Sol. Cells 278 (2024) 113176, https://doi.org/10.1016/j.solmat.2024.113176.

[21] A. Bonk, M. Braun, A. Hanke, J. Forstner, D. Rückle, S. Kaesche, V.A. Sötz, T. Bauer, Influence of different atmospheres on molten salt chemistry and its effect on steel corrosion, : AIP Conf. Proc., AIP Publ. LLC (2018) 090003, https://doi.org/10.1063/1.5067097.

[22] A. Bonk, C. Martin, M. Braun, T. Bauer, Material investigations on the thermal stability of solar salt and potential filler materials for molten salt storage, AIP Conf. Proc. 1850 (2017), https://doi.org/10.1063/1.4984429.

[23] F. Paniccia, P.G. Zambonin, Redox mechanism in an ionic matrix. IV. Catalytic effects of peroxide and superoxide on the oxidation of nitrite by molecular oxygen in molten alkali nitrates, J. Phys. Chem. 78 (1974) 1693–1698, https://doi.org/10.1021/j100610a003.

[24] S. Lyon, T. Richardson, B. Cottis, R. Lindsay, D. Scantlebury, H. Stott, M. Graham. Shreir's Corrosion, 4th ed., Elsevier, 2010.

[25] R. Bradshaw, Oxidation and Chromium Depletion of Alloy 800 and 316SS by Molten NaNO3-KNO3 at Temperatures Above 600°C, (1987), https://doi.org/10.2172/5103265.

[26] A. Palacios, M.E. Navarro, Z. Jiang, A. Avila, G. Qiao, E. Mura, Y. Ding, High-temperature corrosion behaviour of metal alloys in commercial molten salts, Sol. Energy 201 (2020) 437–452, https://doi.org/10.1016/j.solener.2020.03.010.

[27] A. Kruizenga, D. Gill, Corrosion of iron stainless steels in molten nitrate salt, Energy Procedia 49 (2014) 878–887, https://doi.org/10.1016/j.egypro.2014.03.095.

[28] Y. Takeda, K. Nakahara, M. Nishijima, N. Imanishi, O. Yamamoto, M. Takano, R. Kanno, Sodium deintercalation from sodium iron oxide, Mater. Res. Bull. 29 (1994) 659–666, https://doi.org/10.1016/0025-5408(94)90122-8.

[29] H. Mehtani, M. Khan, B.N. Jaya, S. Parida, M. Prasad, I. Samajdar, The oxidation behavior of iron-chromium alloys: the defining role of substrate chemistry on kinetics, microstructure and mechanical properties of the oxide scale, J. Alloy. Compd. 871 (2021) 159583, https://doi.org/10.1016/j.jallcom.2021.159583.

[30] R.A. Rapp, Hot corrosion of materials: a fluxing mechanism? Corros. Sci. 44 (2002) 209–221, https://doi.org/10.1016/S0010-938X(01)00057-9.

[31] P.G. Zambonin, J. Jordan, Chemistry of electron transfer and oxygen transfer in fused salts, J. Am. Chem. Soc. 89 (1967) 6365–6366, https://doi.org/10.1021/ja01000a075.

[32] S. Bell, T. Steinberg, G. Will, Corrosion mechanisms in molten salt thermal energy storage for concentrating solar power, Renew. Sustain. Energy Rev. 114 (2019) 109328, https://doi.org/10.1016/j.rser.2019.109328.

[33] A. Fernández, H. Galleguillos, F. Pérez, Thermal influence in corrosion properties of Chilean solar nitrates, Sol. Energy 109 (2014) 125–134, https://doi.org/10.1016/j.solener.2014.07.027.

[34] G.S. Picard, H.M. Lefebvre, B.L. Tremillon, Use of Impedance Measurements for Studying the Effect of Acidity on the Corrosion of Iron in the Molten Equimolar NaNO3-NaNO2-Mixture, in: ECS Proceedings Volumes, 1987, pp. 1028, https://doi.org/10.1149/198707.1028PV..

[35] A. Bonk, W. Ding, A. Hanke, M. Braun, J. Müller, S. Klein, T. Bauer, Effect of gas management on corrosion resistance in molten solar salt up to 620° C: Corrosion of SS316-types and SS347, Corros. Sci. 227 (2024) 111700, https://doi.org/10.1016/j.corsci.2023.111700.

[36] T. Furukawa, E. Yoshida, Y. Nagae, K. Aoto, The high-temperature chemical reaction between sodium oxide and carbon steel. High Temperature Corrosion and Materials Chemistry, The Electrochemical Society Inc, Pennington, NJ, 1998, pp. 312–323.

[37] I. Singh, U. Sen, The effect of NaCl addition on the corrosion of mild steel in NaNO3 melt, Corros. Sci. 34 (1993) 1733–1742, https://doi.org/10.1016/0010-938X(93)90045-I.

[38] J. Kugai, H. Mine, S. Seino, T. Nakagawa, T.A. Yamamoto, H. Yamada, Effects of sodium nitrate and heat treatment atmosphere on the synthesis of α–NaFeO2 layered oxide, Mater. Chem. Phys. 249 (2020) 122948, https://doi.org/10.1016/j.matchemphys.2020.122948.

[39] Y. Zhang, Solubilities of Cr2O3 in fused Na2 SO 4 at 1200 K, J. Electrochem. Soc. 133 (1986) 655, https://doi.org/10.1149/1.2108648.